National Library of Canada
Bibliothèque nationale du Canada

Canadian Theses Service
Service des thèses canadiennes

Ottawa, Canada
K1A 0N4

NOTICE

The quality of this microform is heavily dependent upon the quality of the original thesis submitted for microfilming. Every effort has been made to ensure the highest quality of reproduction possible.

If pages are missing, contact the university which granted the degree.

Some pages may have indistinct print especially if the original pages were typed with a poor typewriter ribbon or if the university sent us an inferior photocopy.

Reproduction in full or in part of this microform is governed by the Canadian Copyright Act, R.S.C. 1970, c. C-30, and subsequent amendments.

AVIS

La qualité de cette microforme dépend grandement de la qualité de la thèse soumise au microfilmage. Nous avons tout fait pour assurer une qualité supérieure de reproduction.

S'il manque des pages, veuillez communiquer avec l'université qui a conféré le grade.

La qualité d'impression de certaines pages peut laisser à désirer, surtout si les pages originales ont été dactylographiées à l'aide d'un ruban usé ou si l'université nous a fait parvenir une photocopie de qualité inférieure.

La reproduction, même partielle, de cette microforme est soumise à la Loi canadienne sur le droit d'auteur, SRC 1970, c. C-30, et ses amendements subséquents.

NL-339 (r. 88/04) c

Canada

UNIVERSITY OF ALBERTA

A METHOD FOR DESCRIBING THE ARTICULAR SURFACES IN THE HUMAN KNEE JOINT

BY

RICHARD G. HAYNES

A THESIS

SUBMITTED TO THE FACULTY OF GRADUATE STUDIES AND RESEARCH

IN PARTIAL FULFILLMENT OF THE REQUIREMENTS FOR THE DEGREE

OF MASTER OF SCIENCE

DEPARTMENT OF MECHANICAL ENGINEERING

EDMONTON, ALBERTA

SPRING 1991

National Library of Canada
Bibliothèque nationale du Canada

Canadian Theses Service
Service des thèses canadiennes

Ottawa, Canada,
K1A 0N4

The author has granted an irrevocable non-exclusive licence allowing the National Library of Canada to reproduce, loan, distribute or sell copies of his/her thesis by any means and in any form or format, making this thesis available to interested persons.

L'auteur a accordé une licence irrévocable et non exclusive permettant à la Bibliothèque nationale du Canada de reproduire, prêter, distribuer ou vendre des copies de sa thèse de quelque manière et sous quelque forme que ce soit pour mettre des exemplaires de cette thèse à la disposition des personnes intéressées.

The author retains ownership of the copyright in his/her thesis. Neither the thesis nor substantial extracts from it may be printed or otherwise reproduced without his/her permission.

L'auteur conserve la propriété du droit d'auteur qui protège sa thèse. Ni la thèse ni des extraits substantiels de celle-ci ne doivent être imprimés ou autrement reproduits sans son autorisation.

ISBN 0-315-66708-7

Canada

UNIVERSITY OF ALBERTA

RELEASE FORM

NAME OF AUTHOR: RICHARD G. HAYNES

TITLE OF THESIS: A METHOD FOR DESCRIBING THE ARTICULAR SURFACES IN THE HUMAN KNEE JOINT

DEGREE: MASTER OF SCIENCE IN MECHANICAL ENGINEERING

YEAR THIS DEGREE GRANTED: 1991

PERMISSION IS HEREBY GRANTED TO THE UNIVERSITY OF ALBERTA LIBRARY TO REPRODUCE SINGLE COPIES OF THIS THESIS AND TO LEND OR SELL SUCH COPIES FOR PRIVATE, SCHOLARLY OR SCIENTIFIC RESEARCH PURPOSES ONLY.

THE AUTHOR RESERVES OTHER PUBLICATION RIGHTS, AND NEITHER THE THESIS NOR EXTENSIVE EXTRACTS FROM IT MAY BE PRINTED OR OTHERWISE REPRODUCED WITHOUT THE AUTHOR'S WRITTEN PERMISSION.

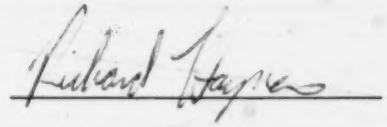

c/o 9744 64-Ave.

EDMONTON, ALBERTA

T6E-0J5

DATE: January 11, 1991.

UNIVERSITY OF ALBERTA

FACULTY OF GRADUATE STUDIES AND RESEARCH

THE UNDERSIGNED CERTIFY THAT THEY HAVE READ, AND RECOMMEND TO THE FACULTY OF GRADUATE STUDIES AND RESEARCH FOR ACCEPTANCE, A THESIS ENTITLED **A METHOD FOR DESCRIBING THE ARTICULAR SURFACES IN THE HUMAN KNEE JOINT** SUBMITTED BY RICHARD HAYNES IN PARTIAL FULFILLMENT OF THE REQUIREMENTS FOR THE DEGREE OF MASTER OF SCIENCE IN MECHANICAL ENGINEERING.

Dr. D. Budney

Dr. D. Steigmann

Dr. M. G. Faulkner

Dr. N. Durdle

Date: January 11/91

For my Mom and Dad

ABSTRACT

The primary goal of this investigation was to establish a method for describing the continuous surfaces of the articular condyles of the knee joint from a finite set of three dimensional data points. The repeatability of the digitizer used to obtain the data was investigated, and its resolution was superior to that used in previous studies. A method for positioning the digitizer to within its resolution was developed. A specimen holding device that did not apply any clamping forces or residual stresses to the specimen was also designed and built. The effect of the amount of input data was investigated, and methods for fitting surfaces through these data were compared.

It was found that smoothing spline fitting of the data was significantly more accurate than least squares fitting, and other methods that have been used previously. The effect of the quantified errors in surface point estimation and slope estimation on the location of the tibio-femoral contact point was also estimated. Using smoothing splines to describe articular joint surfaces, the contact point between two bones can be located to an uncertainty of generally less than 1mm.

ACKNOWLEDGEMENT

The author wishes to thank the many individuals who contributed to this valuable and worthwhile learning experience. Among these are:

- Dr. Budney & Dr. Steigmann for their guidance, without which this project would not have been possible.

- Al Muir, the machinists, and the rest of the technical staff, for their excellent work and assistance.

- Dr. John Cinats for his "Midnight-Special" specimen procurement program, without which my research wouldn't have had a leg to stand on.

- Mr. Andrew Hay for his assistance in intimidating the SUN workstations into running my programs.

- Betty-Ann and Gail for their assistance in formatting and copying this thesis.

And finally, special thanks to Carol for being my inspiration when I needed it the most.

TABLE OF CONTENTS

Chapter 1

1.0 Introduction 1

1.1 Literature Survey 6

1.2 Relevant Surface Geometry Parameters 13

Chapter 2

2.0 Data Acquisition And Processing Equipment 15

2.1 Brown & Sharp Microval Digitizer 15

2.2 Additional Equipment For Data Acquisition 18

2.3 Investigation & Verification Of Digitizer Capabilities 19

2.4 Data Processing Equipment 23

2.4.1 Computer Software & Hardware Cconsiderations 23

Chapter 3

3.0 Shape Description 25

3.1 Methods Of Surface Description 25

3.1.1 Least Squares Bivariate Polynomial Functions 26

3.1.2 Polynomial Splines 27

3.2 Comparison Of Surface Description Methods 31

3.2.1 Accuracy Of 3-D Points & Directional Derivatives 34

3.2.2 Application To Cadaveric Specimens 53

Chapter 4

4.0 Conclusions 56

References 58

Appendix 61

LIST OF TABLES

Table 1. Average T(X,Y) Value for Hemisphere Surface Approximation (no error added to input data) 36

Table 2. Average T(X,Y) Value for Hemisphere Surface Approximation (error added to input data) 36

Table 3. Average Z Error for Hemisphere Surface Approximation (no error added to input data) 37

Table 4. Average Z Error for Hemisphere Surface Approximation (error added to input data) 37

Table 5. Average D Error for Hemisphere Surface Approximation (no error added to input data) 38

Table 6. Average D Error for Hemisphere Surface Approximation (error added to input data) 38

Table 7. Average Error In Smoothing Spline Approximation of Femoral Condyles 51

Table 8. Average Error In Smoothing Spline Approximation of Tibial Condyles . . 51

Table 9. Maximum Distance To Contact Region Boundry for Various Input Grid Spacings 55

Table 10. Normal Vector Error Angle 55

LIST OF FIGURES

Figure 1. Location Of Lateral & Medial Menisci 3

Figure 2. Shape Of The Menisci In A Loaded Knee Joint 4

Figure 3. Shape Of The Menisci In A Flexed & Extended Joint 5

Figure 4. Microval Digitizer With Mounted Specimen 16

Figure 5. Probe Tip With Non-Axial Contact 20

Figure 6. Specimen Fixation Device 21

Figure 7. Surface Plot Of Medial Tibia 33

Figure 8. T(X,Y) As A Function Of Smoothing Factor, Medial Femur 35

Figure 9. Y(X,Y) As A Function Of Smoothing Factor, Lateral Tibia 35

Figure 10. Section Of Quarter Hemisphere For Local Error Examination 39

Figure 11. Local T(X,Y) Value On Hemisphere Section Using Smoothing Splines, 5mm Input Grid (no error added to input data) 40

Figure 12. Local T(X,Y) Value On Hemisphere Section Using Smoothing Splines, 3mm Input Grid (no error added to input data) 40

Figure 13. Local T(X,Y) Value On Hemisphere Section Using Smoothing Splines, 1mm Input Grid (no error added to input data) 41

Figure 14. Local T(X,Y) Value On Hemisphere Section Using Smoothing Splines, 0.5mm Input Grid (no error added to input data) 41

Figure 15. Local T(X,Y) Value On Hemisphere Section Using Smoothing Splines, 0.25mm Input Grid (no error added to input data) 42

Figure 16. Local T(X,Y) Value On Hemisphere Section Using Smoothing Splines, 5mm Input Grid (error added to input data) 42

Figure 17. Local T(X,Y) Value On Hemisphere Section Using Smoothing Splines, 3mm Input Grid (error added to input data) 43

Figure 18. Local T(X,Y) Value On Hemisphere Section Using Smoothing Splines, 1mm Input Grid (error added to input data) 43

Figure 19. Local T(X,Y) Value On Hemisphere Section Using Smoothing Splines, 0.5mm Input Grid (error added to input data) 44

Figure 20. Local T(X,Y) Value On Hemisphere Section Using Smoothing Splines, 0.25mm Input Grid (error added to input data) 44

Figure 21. Local Z Error On Hemisphere Section Using Smoothing Splines, 5mm Input Grid (error added to input data) 45

Figure 22. Local Z Error On Hemisphere Section Using Smoothing Splines, 3mm Input Grid (error added to input data) 45

Figure 23. Local Z Error On Hemisphere Section Using Smoothing Splines, 1mm Input Grid (error added to input data) 46

Figure 24. Local Z Error On Hemisphere Section Using Smoothing Splines, 0.5mm Input Grid (error added to input data) 46

Figure 25. Local Z Error On Hemisphere Section Using Smoothing Splines, 0.25mm Input Grid (error added to input data) 47

Figure 26. Local D Error On Hemisphere Section Using Smoothing Splines, 5mm Input Grid (error added to input data) 47

Figure 27. Local D Error On Hemisphere Section Using Smoothing Splines, 3mm Input Grid (error added to input data) 48

Figure 28. Local D Error On Hemisphere Section Using Smoothing Splines, 1mm Input Grid (error added to input data) 48

Figure 29. Local D Error On Hemisphere Section Using Smoothing Splines, 0.5mm Input Grid (error added to input data) 49

Figure 30. Local D Error On Hemisphere Section Using Smoothing Splines, 0.25mm Input Grid (error added to input data) 49

NOMENCLATURE

Medial,medio-	Denoting a position towards the midline or middle.
Lateral,latero-	Denoting a position away from the midline or middle.
Anterior,antero-	Denoting a position towards the front, or in the front part of.
Posterior, postero-	Denoting a position towards the rear, or in the back part of.
Tibiofemoral	Relating to both the tibia and the femur.
Patellofemoral	Relating to both the patella (knee cap) and the femur.
Condyle	A rounded projection on a bone.
Intercondylar	A location between condyles.
Fossa	General term for a hollow or depressed area, a trench, or a canal.
$Z=f(X,Y)$ $Z(X,Y)$	Polynomial function in the parameters x and y, describing a three dimensional surface.
ϵ	Epsilon, a parameter denoting the amount of error.
C_i	Coefficient of a least squares polynomial fit of data.
λ_i,μ_i	Knot locations of a polynomial spline in directions x and y respectively.
k,ℓ	Degrees of polynomial spline in x and y respectively.
g,h	Number of interior knots in a polynomial spline in directions x and y respectively.
$S(X,Y)$	Polynomial spline fit of surface in parameters x and y to three dimensional data.
$S_s(X,Y)$	Polynomial smoothing spline fit of surface in parameters x and y to three dimensional data.
C_{ij}	Polynomial (or smoothing) spline coefficients.

D_{ij}	Any subrectangle domain within i=0-g, j=0-h.
M(X),N(Y)	Normalized B-splines (Bezier splines) in directions x and y respectively.
$a_{i,q}, b_{j,r}$	Parameters measuring discontinuity in derivatives in x and y directions.
$f_{q,r}$	Tabulated qxr bivariate data.
m_1, m_2	Number of grid lines or data points in directions x and y respectively.
$\delta(c)$	Parameter quantifying closeness of a spline fit to tabulated data.
$\eta(c)$	Parameter quantifying cumulative discontinuity in derivatives.
$\bar{n}_1, \bar{n}_2$	Outward normal vectors to two contacting surfaces at the point of contact.
$\bar{t}$	Tangent plane to a surface at some point.
T(X,Y)	Error parameter quantifying closeness of fit,including both the error in z values and error in derivatives.
Average Z error	The absolute value of the difference between the actual and fitted (either by least squares or splines) Z coordinate at point (X,Y), averaged over many points.
Average D error	The absolute value of the difference between the gradient of a polynomial ($\nabla Z(X,Y)$) and the gradient of a spline ($\nabla S(X,Y)$) evaluated at point (X,Y), averaged over many points.

Chapter One

1.0 Introduction

Increasing human longevity has increased the occurrence of such degenerative conditions as arthritis in the knee joint. Additionally, growing involvement in individual and team sports has caused an increase in the number of knee injuries requiring treatment by orthopaedic surgeons. Sound treatment of these occurrences demands a comprehensive understanding of joint function at both macro and microscopic levels. The function of each individual structure and the interaction between the structures must be understood. Determination of factors which influence the knee's operation most significantly, must necessarily be the first step towards the overall goal of a knee model to predict degenerative conditions, or assist in the assessment and repair of damaged structures.

Early work in this area began in the late 60's with investigation of the forces transmitted across the knee joint. Photoelastic studies [6][22] have been conducted to determine stresses encountered by the bony surfaces. More significantly, with the proliferation of computers and increasing ease of their use in the 1980's, mathematical, numerical, and finite element models of the joint have been attempted.

In general, tensile forces are transmitted across the joint by soft tissues, and compressive forces by the cartilage covered bony surfaces of the tibia, femur, and the patella. The kinematics of the joint are influenced by both the soft tissues (ligaments), and the hard tissues (articular joint surfaces). Ligaments are known to have nonlinear viscoelastic force-extension relations. Frank and Shrive [13] suggest that mechanical

properties vary not only from ligament to ligament, but along the length of the ligament as well. Such information is vital for accurate determination of forces within the joint, but must be combined with an accurate description of joint geometry to be useful.

The menisci in the knee joint have recently become the focus of increasing interest. The menisci are two wedge shaped semi-circular pieces of cartilage that cover a significant area of the lateral and medial condyles of the tibia. As shown in Figure 1, their only attachment points to the tibia are at the anterior and posterior meniscal horns; the rest of the structures can slide smoothly over the condyles. The function of the menisci is to help distribute the compressive load transmitted across the joint. Under compressive loading the menisci deform to match the contours of the femur and tibia, as seen in Figure 2. As the joint flexes, the menisci slide over the tibial condyles, and continue deforming and matching the surfaces as shown in Figure 3. The menisci are no longer casually excised by orthopaedic surgeons as they once were, if found to have been torn or otherwise injured. Total removal of the menisci in the past has been shown to increase the occurrence of arthritis, since contact stresses between the femur and tibia are increased without these structures. Efforts are currently under way to characterize the material properties of the menisci so that it can accurately be included in a mathematical model of the knee joint. With such deformable structures, it is essential that the condylar surfaces are accurately described, since they are the major physical constraints to the locations and shapes of the menisci.

The scope of this thesis involves developing a method for describing the three dimensional geometry of the articular surfaces of the human knee joint. This method

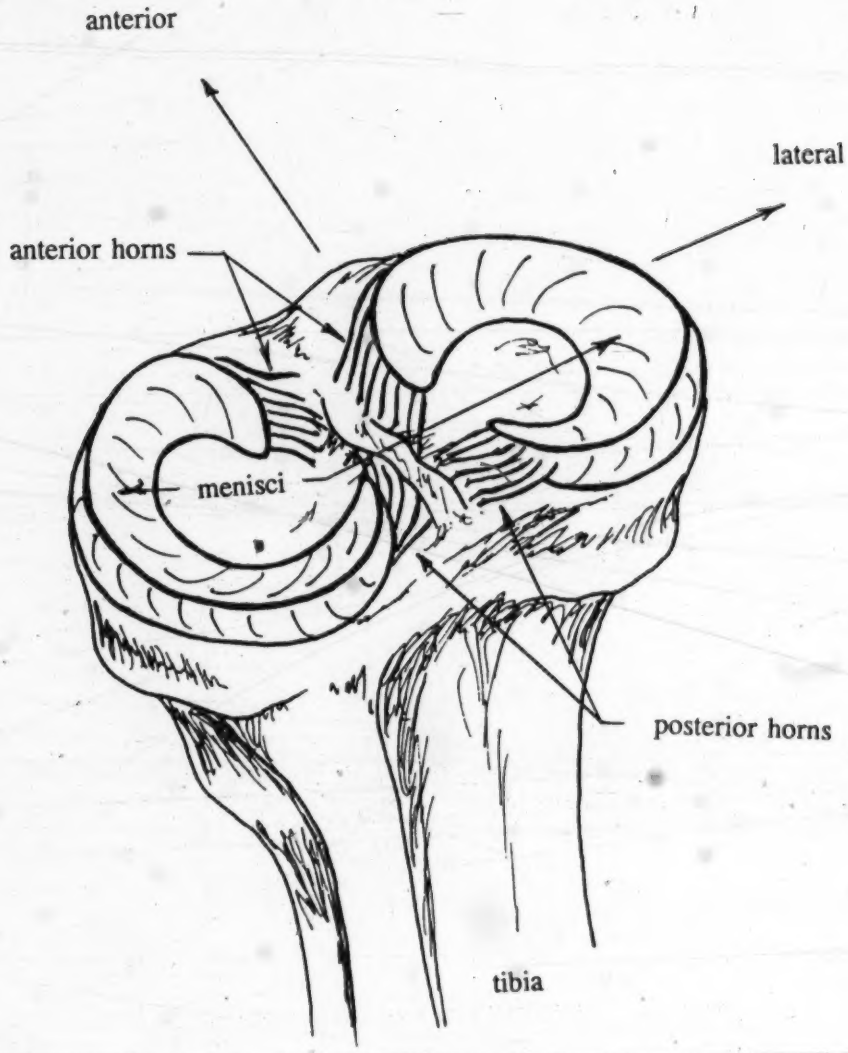

Figure 1. Location of Lateral & Medial Menisci.

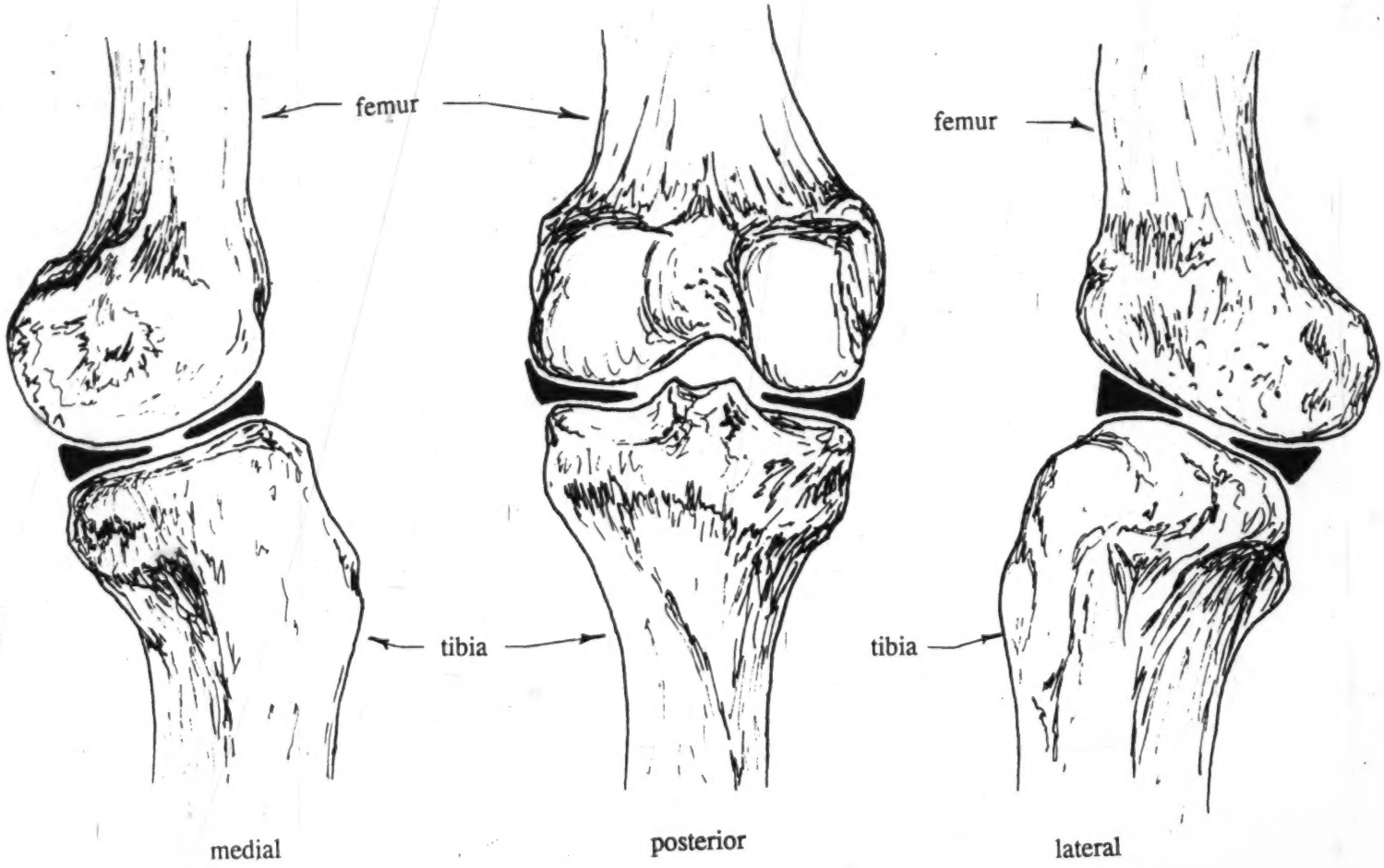

Figure 2. Shape Of The Menisci In A Loaded Knee Joint.

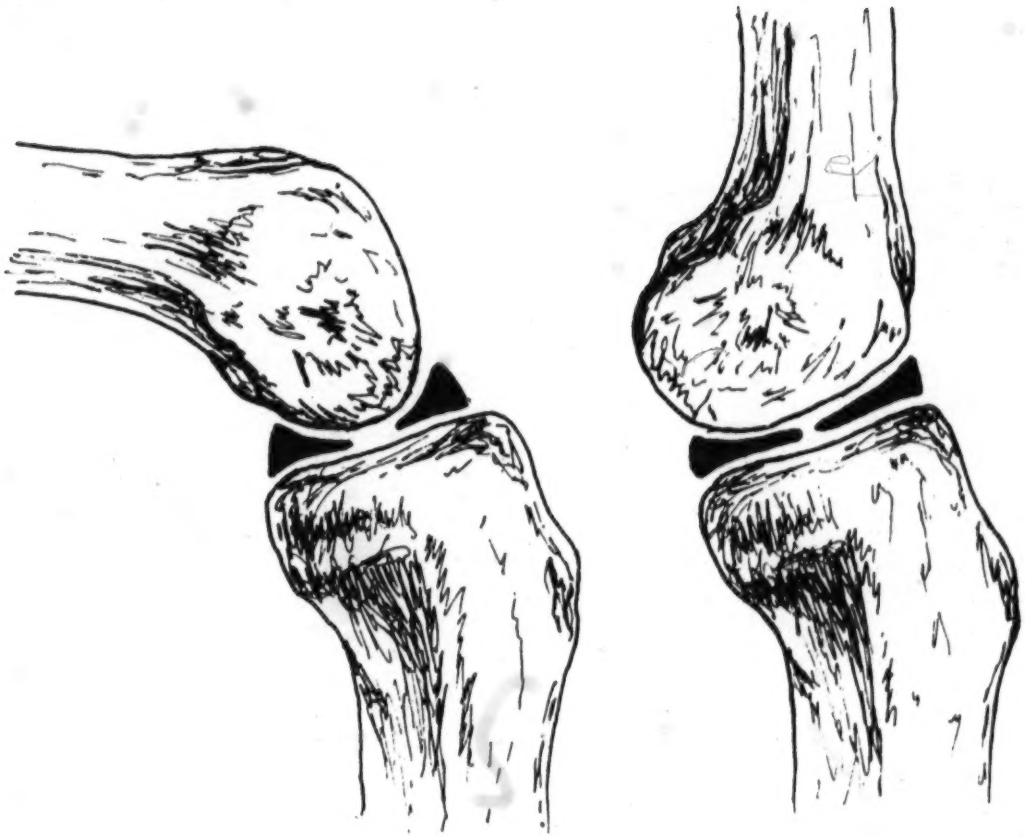

flexed joint

extended joint

Figure 3. Menisci In Flexed & Extended Joint.

will be used to locate the contact point between articular surfaces. Further, accurate description of the articular surfaces may be used as physical constraints to the menisci, allowing for an investigation of their load carrying and sharing capabilities. The method may also be used for describing other joint surfaces (temporomandibular joint for example).

1.1 Literature Survey

Tremendous advances in the past two decades have occurred in understanding and characterizing the structures of the knee joint, their function, and degenerative conditions which they may experience. The scopes of most previous studies have been very specific, to the point of oversimplifying or neglecting important structures like the menisci or ligaments.

The goal of Maquet's [22] two dimensional photoelastic study was to investigate tibio-femoral contact stresses, and thus ignored all structures other than the articular joint surfaces. Accurate geometry of the test specimens was crucial for valid results, but the focus was on reporting stress levels due to loading and specimen geometry, not detailed description of the articular surfaces. Chand et al.'s [6] photoelastic three dimensional stress distribution investigation included a 3.175mm (1/8 inch) thick layer of foam rubber between the surfaces to simulate the load sharing of the menisci. Similarly, Chand et al. were concerned with levels of stress in the joint, not with an analytical method of describing the joint surfaces.

Frankel et al.'s work in 1971 [14] was concerned with diagnosing internal

derangement of the knee through non-invasive methods. Gait analysis was performed in hopes of finding macroscopic motion changes due to internal damage. Specifically, changes in the path of the femoral instantaneous center of rotation through the gait cycle was investigated as being symptomatic of tissue damage. Articular surface geometry as such was not considered, but motions of specific points on the femur were tracked using serial x-rays to locate the femoral instantaneous center of rotation. Placement of the joint with respect to the x-ray plate and the x-ray source influences the size, clarity, and the actual shape of the resulting image [19]. Subjective decisions were made in locating the relevant points and determining the location of the perpendicular bisector of the segment connecting the points. The prime consideration was detecting "abnormal" motion of the instantaneous center of rotation in an abnormal joint.

Similarly in Reilly and Marten's [32] investigation of quadriceps muscle forces and patellofemoral joint reaction forces, photographs were analyzed subjectively to determine overall joint geometry. Also worthy of note is that this is not a three dimensional model of the joint, but a sagittal one.

Matthews et al. [24] were interested in load bearing in the patellofemoral joint, and also used x-ray techniques. In this cadaveric study, thin radiopacque metal markers were secured to ligament insertion points for better contrast in the x-rays. Directions were determined visually and graphically from the x-rays as well. Dyes were used to determine the bounds of the contact region, and the mechanical function of the patella was idealized as a frictionless pulley.

Andriacchi et al. [2] addressed nonlinear material characteristics and deformations

in a finite element model. Of six potential regions of contact, this model chooses the "appropriate" one through the correct assumption that contact regions are only capable of resisting forces perpendicular to the surface. This assumption is valid as Radin and Paul [30] showed the coefficient of friction in the joint, lubricated with synovial fluid to be extremely low. The implication of this low coefficient is that the shear force generated between the two surfaces is negligible, hence all force must be normal to the surface. Twelve hydrostatic elements which could only resist forces perpendicular to their surfaces represented the contact surfaces, and were arranged in two rows on the medial and lateral condyles. Each "hydrostatic element" was a three dimensional eight node brick element, with four nodes attached to the tibia, and four to the femur. The criterion of nearest common perpendiculars of surface normals between the tibia and femur was used to determine at which element in each row contact occurred. Results of the study indicated the importance of the joint surface geometries and particularly the menisci, without which it was claimed the joint could not be stabilized against antero-posterior and medio-lateral deflections, or against buckling under loads of more than 10% of body weight.

Knee prosthesis design focuses on replacement of diseased, worn, or damaged articular surfaces with minimal disruption of ligamentation and musculature. Goodfellow and O'Connor [16] addressed the dilemma of design rationale. Allowing the contact components to distribute the load over large contact areas reduces contact stresses, but at the expense of limiting natural physiological motion. Spheres in spherical sockets would fit one another in all positions of the joint, and thus provide large areas of contact.

However if the knee joint was replaced on both medial and lateral sides by such devices, it would be restricted from six degree of freedom motion to only one: rotation about the flexion-extension axis. Such a solution would eliminate the need for load sharing structures like ligaments since motion would be completely controlled by the sockets. Not only does this restrict the joint's range of motion, but it causes a drastic change in the way it is loaded. Whereas the articular surfaces, menisci, and ligaments share the load in a healthy knee, the entire load is transmitted through the sockets with this type of replacement. This may cause loosening and failure of the prosthesis within as little as 5 years [27]. Conversely designs which allow rolling, translation, and distraction of the joint surfaces will typically have smaller contact areas and thus higher stresses, which puts greater demands on construction materials from a wear and fatigue point of view. Clearly, the more anatomically correct the prosthesis, the more advantageous from both points of view. Accurate knowledge of the physical size and shape of the articular surfaces is therefore crucial to the design of knee replacement prostheses.

An attempt at describing the overall dimensions of the femoral condyles relevant to implant design was presented by Wyss et al. [36]. A pantograph method was used to record the shape of the femoral condyles. The necessity for three dimensional representation of the femur was foreseen, and pantograph recordings were made at various levels (between 5 and 10 mm increments) on the condyles to achieve this. Moisture sensitivity of the cartilage was recognised, and the cadaveric specimens were sufficiently soaked in Ringer solution to allow swelling of the cartilage to original size. Typical recording graphs contain unexpected discontinuities. Only gross dimensions

were determined from the graphs; no equations were fitted through the data.

Wismans et al.'s [34] three dimensional mathematical model of the knee joint required accurate three dimensional representation of the tibial and femoral surfaces for its solution technique. In this study 50 to 100 three dimensional data points were recorded on each condyle using a dial gauge apparatus. The radius of the dial gauge end was corrected for, and the deformations of the cartilage layer were ignored due to their small (<0.1mm) magnitude. Bivariate least squares polynomials of orders 3 and 4 were calculated for the condyles of the tibia and femur respectively, and a standard deviation was stated as 0.5mm. Evaluation and differentiation of the polynomial expressions to determine tangent planes and surface normals were implemented to determine the contact locations on the tibia and femur. This insightful approach also used non-linear force extension relations for the ligaments, and solved for joint reactions as a function of external loading and flexion angle.

Unfortunately the accuracy of this model is suspect since its representation of the articular surfaces has been smoothed to such a degree (0.5 mm standard deviation). It was not explicitly stated what this standard deviation referred to: coordinate measurements, or fitting of the surface with bivariate polynomial functions. Such significant errors in the estimation of the surface profiles may lead to large errors in the computed direction of the surface normal, incorrect joint geometry, and erroneous muscle and reaction forces. The menisci were neglected, thus their load sharing capacity was not considered. This method did simplify the solution technique, but at the expense of accuracy.

Dial gauges attached to a probe indicated the coordinate values of surface points in Wismans' study. An algorithm was also used to correct for the radius of the probe tip. Certainly though, there must have been a subjective decision made as to when "contact" occurred between the probe and articular surface. This judgement of "contact" may not have been consistent for all the data points recorded. As well, error may have been introduced in the recorded values since interpreting readings between graduations on a dial gauge is subjective.

Rehder [31] used a more systematic approach in his morphometric study of the femoral condyles. He successfully described surface sections as involutes of a circle, Archimedean, and logarithmic spirals. Curvature of the surfaces was calculated to the claimed accuracy of measurement of 0.2mm. Slices through the femur 4mm thick were procured, and X,Y-coordinates of the cartilage surface were obtained using a semiautomatic image analyzing system (Kontron) and a H.P. 9815 computer. While the accuracy of this method is better than that of Wismans', it fails to address the three dimensional nature of the condyles in a manner advantageous to anything other than a planar model of the joint. It is unlikely that this method can be adapted to a Wismans' type model because it uses finite width slices, and thus cannot provide continuity of derivatives across these slices.

Accuracy of measurement of articular surface point coordinates is fundamental to an accurate and anatomically correct mathematical description of these surfaces. Rehder's claimed measurement accuracy using an image analysis method is 0.2mm. Again this is based on 4.0mm thick sagittal slices through the femur, and thus the three

dimensional data obtained is not for an infinitely thin plane, but averaged over the 4.0mm.

Studying control of rolling and sliding at natural joints, Wongchaisuwat et al. [35] modeled the surface of the femur as an ellipse, and the surface of the tibia as a flat plate. This study is primarily concerned with muscular control of motion of the joint, for which accuracy of joint geometry was not a primary concern.

The model proposed by Mikosz et al. [25] drew on the work of Iseki and Tomatsu [18] for determination of the tibio-femoral contact points. Iseki and Tomatsu determined contact regions between the tibia and femur for discrete flexion angles through a method where silicon rubber was injected into cadaveric knees with soft tissues intact. Contact points were determined for six discrete flexion angles (-8,5,15,30,60,90 degrees). For any angle other than these, the real contact point was approximated by the nearest of the six angles; the contact point does not move continuously with continuous flexion as seen physically, it moves in a stepwise fashion. Mikosz et al. imposed further constraints such as maximum physiological muscle force on the model. Muscle forces were chosen on a random basis subject to physiological constraints, and the solution considered valid when both the constraints and equilibrium equations were satisfied.

Zoghi et al. [37] recognise that little work had been done in describing the geometric variation in three dimensions of the knee joint. Their paper used a generalized reduced gradient optimization method for describing the medio-lateral shape variation of sagittal sections through the formalin preserved human distal femurs. Surface topography of slices taken 3.175mm (1/8 inch) apart was measured using a six degree of freedom

commercial measuring device. Lateral and medial condyle slices were reconstructed using two and three circular arcs respectively, and the intercondylar fossa by two circular arcs connected by a line segment. They concluded that the condyles and intercondylar fossa could be described by sections of spheres, cylinders, oblique cylinders, and cones, to an uncertainty of 1mm. Though this may be a simple way to describe the condylar surfaces, an accuracy of 1mm is not acceptable.

As a result of the number of mechanisms which act across human joints (several ligaments and several muscles), equilibrium equations are generally statically indeterminate. Several optimization techniques based on value judgements and assumptions have been used to solve these problems. Baragar & Osborne [3] and Osborne & Baragar [28] attempted to minimize joint loading, and optimized bite force for assumed muscle loading in their mandibular studies. An et al. [1] have also used a method focused on minimizing the upper bound of muscle stress to obtain unique solutions for loading of the elbow. Hence using physiologically based assumptions to determine valid optimization criteria, the apparently indeterminate problem can be rendered tractable.

1.2 Relevant Surface Geometry Parameters

The objective of this investigation is to provide a method for describing the three dimensional geometry of (various) articular joint surfaces, specifically that of the knee, to a high degree of accuracy. At the very least, it must be possible to locate any three

dimensional point on the surface of a condyle. A representation was attempted in Wismans' model by using bivariate least squares polynomials calculated from a finite number of digitized data points. The least squares method is not acceptable for this application because it smooths the data too much, yielding a surface that is not anatomically correct. In this thesis a method has been developed to describe the articular joint surfaces continuously, and to a high degree of precision.

Several authors have correctly recognised that due to the extremely efficient lubrication of the joint, the articular surfaces cannot support shear forces. Consequently contact forces must be normal to both surfaces in contact. The direction of the normal to the surface at any point can be calculated as the vector cross product of two surface tangents at the same point. Collinearity of surface normals was a constraint used by Wismans to locate the tibio-femoral contact point, and the method developed in this investigation is capable of determining surface tangents in two orthogonal directions at any point within the domain.

Chapter Two

2.0 Data Acquisition and Processing Equipment

The digitizer used in this investigation is shown in Figure 4, complete with a mounted specimen. The digitizer employs a probe load cell which triggers the acquisition of three dimensional data, thus eliminating subjectivity from the process. Elaborate data processing equipment was not required; a personal computer and networked Sun 3/60 workstation were used, and the emphasis was on evaluation of appropriate software to process 3-D data points into the desired representation of the surfaces. Software was developed to define points on the articular joint surfaces, and evaluate two orthogonal derivatives at arbitrarily chosen points. This software could be used by itself, or could be modified and incorporated into a comprehensive knee model.

2.1 Brown & Sharp Microval Digitizer

A Brown & Sharp Microval digitizer was used in this investigation to obtain the necessary three dimensional data. This machine is primarily used for precise measurement of industrial machine components and verification of their specifications. Physically the digitizer is quite massive at .75m X .75m X 1.3m, and 150kg, and its rigidity is sufficient to enable deflections due to probe or positioning forces to be neglected.

The digitizer employs a right-handed Cartesian coordinate system, with an X-Y plane defined by its granite worktable surface. The measuring range is 356mm X 406mm X 305mm in the X,Y, and Z directions respectively, with a measurement

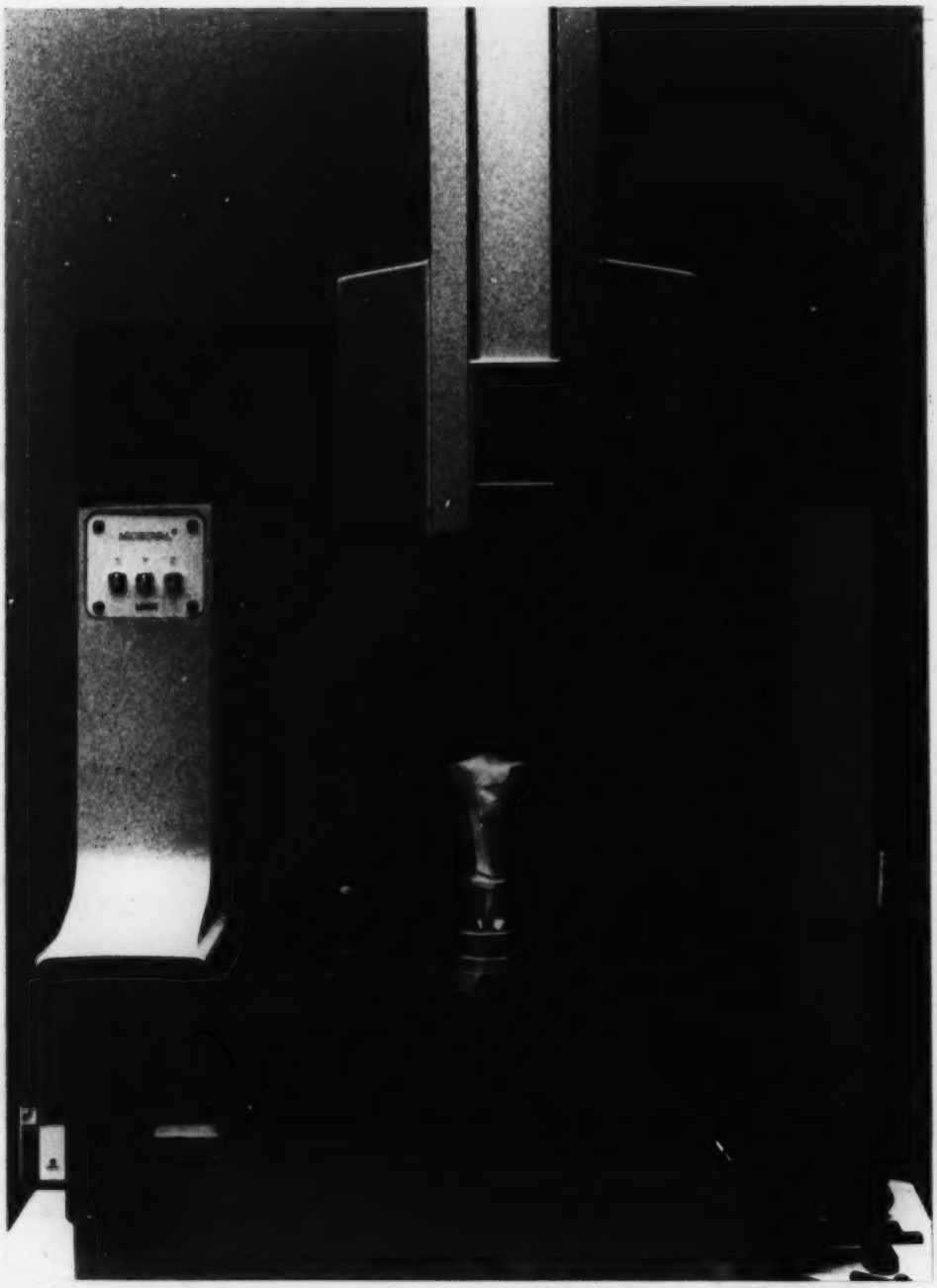

Figure 4. Microval Digitizer With Mounted Specimen.

resolution of 0.002mm along each axis. Linear motion along each axis is permitted with air bearings, each of which has an independent shut-off valve. Thus motion along only a single axis can be achieved by shutting off the air supply to the remaining axes' bearings. Position measurement is achieved through the use of an "opto-electrical" procedure which reads incremental scale divisions along glass scales firmly mounted in recesses in each of the axis rails.

Factory supplied probes consist of a slender shaft of approximately 2mm diameter and 40mm length. A 4mm sphere is mounted on the tip, and the probe base is threaded to fit into a load cell that measures probe tip forces. The load cell measures force in the X-Y plane as well as in the -Z direction. The load cell automatically triggers acquisition of X,Y, and Z coordinates of the point of contact on the sphere when the probe tip force exceeds a preset value (5g-50g sic.). An internal algorithm monitors load cell output at the instant of acquisition, and can thus determine the location on the surface of the sphere that made contact. Hence the displayed coordinates are those of the actual point of contact, not of the center of the probe tip.

A 19.05mm (3/4 inch) requalification sphere is rigidly attached to the granite worktable, and is used on start-up of the digitizer to initialize its origin. The probe tip must be struck against the requalification sphere a minimum of four times at start-up. Through processing output from the axes' linear sensors and the probe load cell for each strike, the digitizer has been programmed to determine the location of the probe with respect to the digitizer's origin, as well as calculating the diameter of the probe tip. Points may then be measured relative to the digitizer's origin. An origin on a specimen

may be defined through a series of strikes on its surface, and then all measurements made relative to the specimen origin.

2.2 Additional Equipment For Data Acquisition

Several specialized items were required for the specific application of digitizing articular joint surfaces. With a resolution of 0.002mm, it was necessary to develop a means to position the probe accurately and repeatably to such small increments. This was achieved through the use of a pair of Mitutoyo 0-25mm micrometers. The two micrometers were mounted so as to induce translations of the probe in X and Y directions independently. The accuracy of the micrometers is not relevant since they were used simply to move the probe in very small increments. Digital readout from the digitizer was used to ascertain its position, and when the desired location along an axis was achieved the appropriate air bearing was turned off to prevent any subsequent motion. Using this method the probe could be positioned to an accuracy smaller than that of the readout (<0.001mm).

It was necessary to design a new probe tip for digitizing articular joint surfaces. Some of the data processing routines required that data points were taken on a rectangular grid. Using the factory supplied probe with the 4.0mm spherical tip, contact with a non-level surface would not occur along the probe's axis of symmetry. Ideally a sharply pointed tip would totally eliminate this type of error, but it might possibly pierce the articular cartilage before sufficient force to trigger data acquisition was generated. By reducing the tip diameter to 0.5mm, the occurrence of non-axial contact

is virtually eliminated, even with the continuously varying slope of the articular surface. A 0.5mm glass sphere (from sandblasting stock) was bonded to the tip of a 0.5mm diameter stainless steel tube as shown in Figure 5, and was sufficiently rigid that deformations under the expected loads were negligible.

To assure rigid fixation of the specimen during the digitizing process a specimen holding device was designed and used as shown in Figure 6. A threaded rod was embedded into a 38.1mm (1-1/2 inch) steel ball, which was mounted between cup shaped steel disks mounted to a 9.525mm (3/8 inch) aluminum plate. An aluminum specimen mounting spindle screwed on to the rod at one end, and was tapped for a 6.35mm (1/4 inch) thread at the other end. The aluminum plate was bolted to the granite worktable using four of the 9.525mm tapped holes in its surface. A 6.35mm bolt was bonded into the femur/tibia using bone cement, and the bolt then screwed into the specimen spindle. Since the bone was not clamped, no stresses or resulting time dependent deformations were induced in it. The specimen could be arbitrarily oriented, and then locked in place by tightening bolts which squeeze cupped disks together. This gave a large range of possible orientations, and was observed to be sufficiently stiff to resist probe forces without detectable deformations.

2.3 Investigation & Verification of Digitizer Capabilities

A stationary rigid surface was required for verification of the digitizer's capabilities. Two high quality steel ball bearings, 50.8mm (2 inches) and 25.4mm (1 inch) in diameter respectively, were rigidly bonded to an aluminum plate. The ball

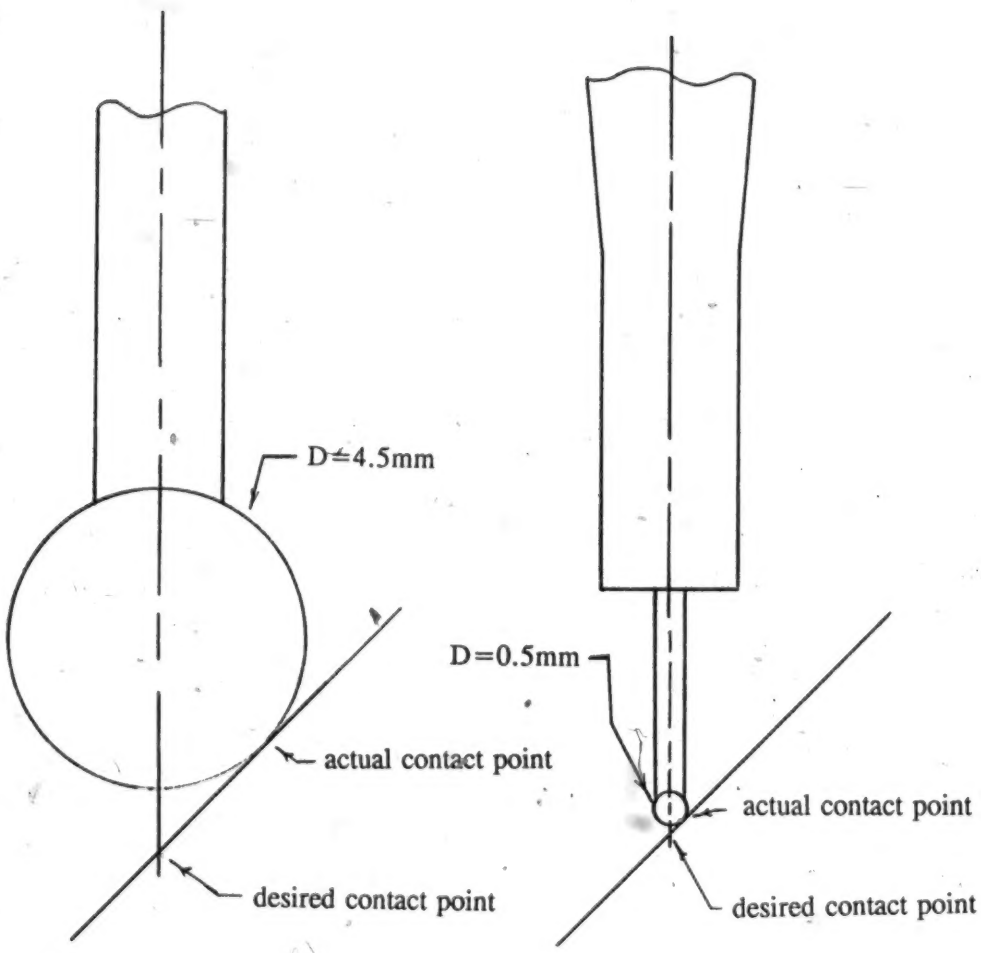

Figure 5. Probe Tip With Non-axial Contact.

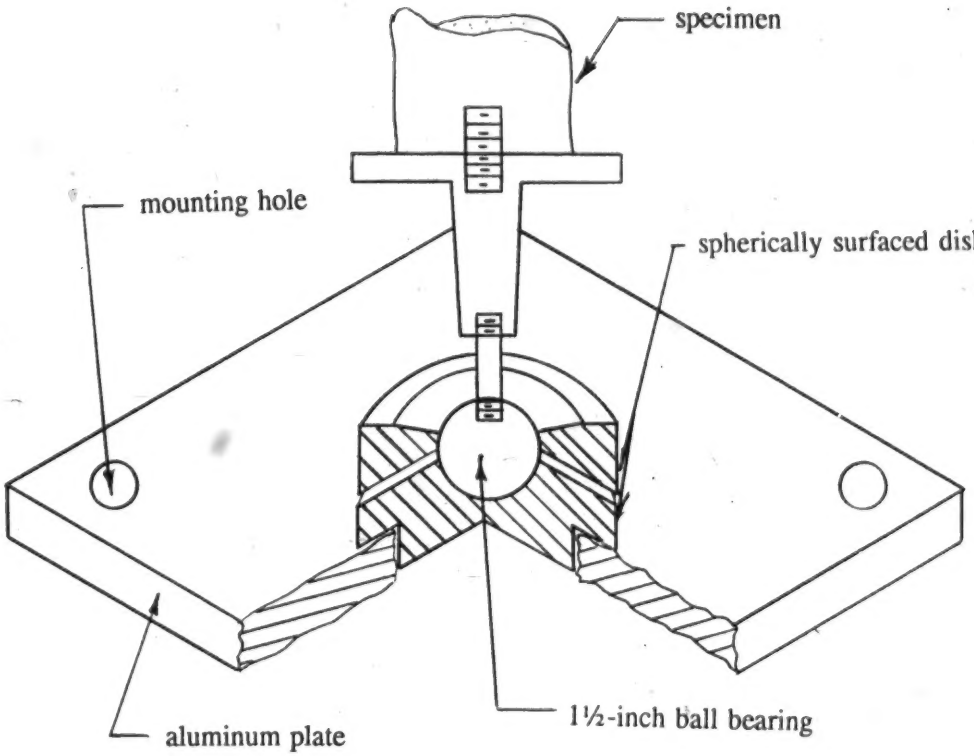

Figure 6. Specimen Fixation Device.

bearings presented similar radii of curvature to some regions on the articular joint surfaces. The aluminum plate was bolted to the digitizer's granite worktable in the same manner as the specimen mounting plate. Repeated measurements were then taken at various points on the ball bearings, and the results analyzed statistically.

Repeated digitizing of the same point without repositioning in the X-Y plane revealed that the slope of the surface has an effect on the measurement obtained. Where the bearing surface was nearly level, the standard deviation of the measurement was approximately 0.0016mm or 1.6 microns. Closer to the waist of the bearing, where the surface inclination was approximately 60 degrees, standard deviation was on the order of 6 microns. Measurements appeared insensitive to radius of curvature; slope was the main influence.

Repeated digitizing of the same point including X-Y repositioning for each measurement indicated that measurements were not sensitive to repositioning of the probe in the X-Y plane. In this study, a standard deviation of approximately 2 microns to 5 microns was also observed for similar cases as above. Hence it was concluded that X-Y repositioning had no significant effect on the magnitude of measurement error. The measurement error was assumed to be normally distributed, and at the .001 level of significance a maximum error estimate was calculated to be 4 microns. This analysis of data from these investigations indicates the real accuracy that can be expected in measuring coordinates from articular joint surfaces by a knowledgeable but not highly trained user, and is not just a listing of manufacturer specifications.

2.4 Data Processing Equipment

The method developed here can be implemented on a personal microcomputer, elaborate processing equipment is not required. Some work was done on a Sun 3/60 workstation, but could also have been done on a microcomputer. A primary consideration was ease of input/output. It is assumed that three dimensional data will be provided on floppy disk, as it is much too voluminous and tedious to enter manually each time the program is run. A line printer was also used for obtaining hard copies of results.

2.4.1 Computer Software & Hardware Considerations

The routines developed in this investigation were written in Microsoft QuickBASIC 4.5, and standard Fortran 77. QuickBASIC was chosen for its convenience. Fortran 77 was used because an available software package for surface fitting with variable smoothing was written in that language, and was simply too large to bother converting to another language. Fortran has the advantage of being computationally quicker when compiled, but is less user friendly, and more difficult to debug. Neither has significant advantages or disadvantages, but converting routines from one language to the other could be time consuming and tedious.

Necessary hardware is to some extent dependent on the perceived needs of the user. All routines developed here will run on a IBM compatible microcomputer, but if Fortran is chosen, it is advisable to use a computer equipped with a 386 microprocessor and a math coprocessor to reduce processing time. At minimum, a floppy drive for

program input/output is essential and a hard drive would be more useful. If these routines are used as a subroutine in a larger program (such as a comprehensive knee model) it is probable that such hardware requirements will have already been met, and additional hardware is not required.

Chapter Three

3.0 Shape Description

The problem faced, is that of describing an infinite number of surface points and the slope at each point by a finite, manageable number of independent variables derived from a finite sample of the surface points. This can be achieved by expressing the surface as a function above a plane such as $Z = f(X,Y)$. The functions describing the surfaces must be investigated graphically to ensure their anatomical correctness. Differentiation of the functions with respect to X and Y is not difficult, and will produce two vectors for which the cross product will be the vector normal to the surface at that point. The surface could equally be defined in cylindrical or spherical coordinates, but no advantage is foreseen since the surfaces are not extensively symmetric. Location and orientation of the coordinate axes can be chosen advantageously in consideration of anatomical features such as long axes of bones and the flexion axis of the joint. The resulting functions must be investigated visually and analyzed to ensure that the surfaces appear anatomically correct and are free from discontinuities.

3.1 Methods of Surface Description

Consistent with the above argument, methods for fitting data to bivariate functions were investigated. A right handed cartesian coordinate system was chosen, which was also consistent with the digitizer's coordinate measurement system. Least squares fitting of third and fourth order bivariate polynomials and fitting with spline functions were investigated for describing the surfaces. Spline functions are piecewise continuous

functions valid in subregions of the total domain under consideration. Constraints such as continuity of derivatives are imposed at the boundaries of the subregions (knots of the spline) to link the functions. Different types of splines including interpolating, smoothing, and least squares splines were investigated.

3.1.1 Least Squares Bivariate Polynomial Functions

Least squares fitting of bivariate polynomials is a simple extension of least squares curve fitting. In the curve fitting problem, it is desired to determine the coefficients C_i of a polynomial function of degree P, namely

$$y = C_0 + C_1x + C_2x^2 + \cdots + C_px^p \qquad (1)$$

which approximates the underlying nature of the data. For a given number of data points (x_i,y_i) i=1,2,...,n, the sum of squares error in this approximation can be written as:

$$\epsilon = \sum_{i=1}^{n} [y_i - (C_0 + C_1x_i + C_2x_i^2 + \cdots + C_px_i^p)]^2 \qquad (2)$$

To minimize the error, equation (2) is differentiated with respect to each C_i i=0,1,...,p (p+1 times), and set equal to zero. The resulting system of equations can be solved using a Gaussian elimination technique for the coefficients C_i. This method can be used for fitting a surface to three dimensional data by replacing equation (1) with a bivariate polynomial function of degree 2 (for example) in x and y such as:

$$z = C_0 + C_1x + C_2y + C_3xy + C_4x^2 + C_5y^2 \qquad (3)$$

A sum of squares expression analogous to equation (2) can be written for equation (3), and solved in a similar manner. It should be noted that the analytical expression for the data is an approximation which minimizes the error; it is not necessarily an accurate representation of the underlying function. That is to say, the calculated surface function approximates the data with the minimum error over the domain, but the surface may not pass through any of the data points. Thus the surface may or may not be accurately represented by the calculated least squares polynomial function.

3.1.2 Polynomial Splines

In their purest form, polynomial interpolating splines fit piecewise polynomials through the data points. This eliminates such smoothing of the data as seen with least squares fitting where the polynomials may not fit through any of the data at all. This has the unfortunate drawback of misrepresenting the underlying function if measurement error is present in the data being fitted. Derivatives of this spline would show unacceptable deviations from those of the underlying function since fitting through data with measurement error would make the spline approximation fluctuate above and below the surface of the underlying function.

Least squares splines fit least squares polynomials to subregions of the domain, and still impose continuity constraints at the boundaries of the subregions. Since the least squares method is used, it is again possible that the resulting mathematical surface will not pass through any of the data points, as with simple least squares fitting. Conversely, since numerous subregions are subjected to least squares fitting it is reasonable to expect

better representation of localized surface features than with a simple least squares fit which fits the entire domain by a single function, smoothing localized features too greatly. Smoothing splines are a compromise between interpolating and least squares splines. Correct adjustment of the amount of smoothing permits the user to "filter out" measurement error or noise in the data without smoothing the data excessively.

A general algorithm for determining the coefficients of a bivariate spline is presented well by Dierckx [8]. For fitting a surface on a closed rectangular domain D=[a,b]x[c,d], consider the increasing sequence of real numbers:

$$a = \lambda_0 < \lambda_1 < \cdots < \lambda_{g+1} = b,$$

$$c = \mu_0 < \mu_1 < \cdots < \mu_{h+1} = d. \qquad (4)$$

Then a function S(X,Y) is said to be a spline of degree k in x and ℓ in y, with knots λ_i, i=1,2,...,g in the x-direction and μ_j, j=1,2,...,h in the y-direction if the two following conditions are satisfied:

(i) s(x,y) is given by a polynomial at most of degree k in x and at most ℓ in y on any subrectangle:

$D_{ij} = [\lambda_i,\lambda_{i+1}]x[\mu_j,\mu_{j+1}]$, i=0,1,...g, j=0,1,...h.

(ii) Within the domain D all derivatives $\partial^{i+j}s(x,y)/\partial x^i\partial y^j$ subject to $0 \le i \le k-1$ and $0 \le j \le \ell-1$ are continuous.

If the additional knots:

$$\lambda_{-k} = \lambda_{-k+1} = \cdots = \lambda_{-1} = a,$$

$$b = \lambda_{g+2} = \cdots = \lambda_{g+k} = \lambda_{g+k+1},$$

$$\mu_{-\ell} = \mu_{-\ell+1} = \cdots = \mu_{-1} = c,$$

$$d = \mu_{h+2} = \cdots = \mu_{h+\ell} = \mu_{h+\ell+1},$$

are introduced, then every such spline has a unique representation of the general form:

$$s(x,y) = \sum_{i=-k}^{g} \sum_{j=-\ell}^{h} c_{i,j} M_{i,k+1}(x) N_{j,\ell+1}(y)$$

where $M_{i,k+1}(x)$ and $N_{j,\ell+1}(y)$ are B-splines in the variables x with knots located at $\lambda_i, \lambda_{i+1}, \ldots, \lambda_{i+k+1}$, and y with knots located at $\mu_j, \mu_{j+1}, \ldots, \mu_{j+\ell+1}$. The $M_{i,k+1}(x)$ and $N_{j,\ell+1}(y)$ have the property that

$$M_{i,k+1}(x)=0 \text{ if } x \le \lambda_i \text{ or } x \ge \lambda_{i+k+1},$$

and

$$N_{j,\ell+1}(y)=0 \text{ if } y \le \mu_j \text{ or } y \ge \mu_{j+\ell+1},$$

and are capable of being evaluated in a stable manner. Further, S(X,Y) becomes a single polynomial in D if the discontinuities of the k-th derivative in x and the ℓ-th derivative in y at the interior knots λ_q and μ_r all vanish, that is,

$$\sum_{i=-k}^{g} a_{i,q} c_{i,j} = 0, \quad q = 1,2, \cdots, g, \quad j = -\ell, -\ell+1, \cdots, h \qquad (5)$$

and

$$\sum_{j=-\ell}^{h} b_{j,r} c_{i,j} = 0 \quad r = 1,2, \cdots, h, \quad i = -k, -k+1, \cdots, g, \qquad (6)$$

where the coefficients $a_{i,q}$ and $b_{j,r}$ are given by:

$$a_{i,q} = M_{i,k+1}^{(k)}(\lambda_q + 0) - M_{i,k+1}^{(k)}(\lambda_q - 0),$$

$$b_{j,r} = N_{j,t+1}^{(t)}(\mu_r + 0) - N_{j,t+1}^{(t)}(\mu_r - 0).$$

Thus, for a given set of values $f_{q,r}$ at the grid points (x_q,y_r), for $q=1,2,\ldots,m_1$, $r=1,2,\ldots,m_2$, on a rectilinear mesh within the rectangular domain [a,b]x[c,d] it is desired to determine the spline approximation which satisfies the two following criteria:

(i) the spline approximation fits the given data values closely enough,

(ii) the spline approximation is sufficiently smooth, that is, the discontinuities in the spline's derivatives are sufficiently minimized.

These two criteria are expressed mathematically by Dierckx using two separate parameters. Similar to least squares fitting, a parameter quantifying the closeness of fit can be defined as:

$$\delta(\bar{c}) = \sum_{q=1}^{m1}\sum_{r=1}^{m2}\left[f_{q,r} - \sum_{i=k}^{g}\sum_{j=t}^{h} c_{i,j}\,M_{i,k+1}(x_q)\,N_{j,t+1}(y_r)\right]^2.$$

A parameter quantifying the cumulative discontinuity of derivatives was derived using equations (5) and (6) and is of the form:

$$\eta(\bar{c}) = \sum_{q=1}^{g}\sum_{j=t}^{h}\left(\sum_{i=k}^{g} a_{i,q}c_{i,j}\right)^2 + \sum_{r=1}^{h}\sum_{i=k}^{g}\left(\sum_{j=t}^{h} b_{j,r}c_{i,j}\right)^2.$$

Hence the problem is to minimize $\eta(\bar{c})$ with the constraint that $\delta(\bar{c}) \leq S$ in which S is a user chosen parameter which controls the amount of smoothing the spline is subjected to. The solution technique has been adapted for maximal computational efficiency, and the details of it are beyond the scope of this thesis. Also beyond the scope of this thesis it can be shown that as $S\to\infty$, $S_s(X,Y)$ becomes a least squares spline, and as $S\to 0$, $S_s(X,Y)$ becomes an interpolating spline.

The algorithm automatically determines the location and number of knots for the spline, and several comments are warranted here. Additional knots are added at locations and in directions where the fit with the data is not sufficiently close. The local addition of these knots limits increases in computational time, and more importantly, additional memory requirement.

This algorithm is particularly well suited to the problem of describing articular joint surfaces from data that contains digitizing error. The smoothing parameter can be adjusted to filter out the digitizing error effectively, but not at the expense of smoothing the data to the extent that it is no longer representative of the articular surface. Therefore this method provides superior accuracy in calculating both surface point coordinates, and directional surface derivatives, and thus surface normals.

3.2 Comparison of Surface Description Methods

The accuracy of surface fitting was compared for a third order, and a fourth order least squares fit, and smoothing spline fit. Data representing surface coordinates of a hemisphere with and without simulated digitizing error were generated. These data were then used as input to the three above stated types of fits, and the accuracy of point and derivative estimation quantified and compared. The accuracy of approximation was also investigated for smoothing splines, on the medial and lateral tibial and femoral condyles.

Measurement of surface points from specimens is quite straightforward, but measuring the slope of the surface in two directions (or even one direction) at a randomly chosen point is not practically possible at present. Thus it is impossible to use only

digitized data from a specimen for a comparison of the accuracy of the various surface fitting methods. To overcome this problem, artificial surfaces were created on which the derivatives could be analytically evaluated. These surfaces were created by fitting least squares bivariate polynomials to digitized data from specimens. The surfaces were then plotted 3-dimensionally to verify their similarity to real specimens. A typical plot is shown in Figure 7. Approximately 150-200 data points were used over an area of at least 800 square mm on each condyle in each polynomial fit. The resulting polynomials allowed evaluation of surface derivatives in two orthogonal directions in a simple manner. The polynomials were evaluated on a rectangular grid, and random error with known mean and standard deviation was then added to the Z coordinate to simulate measurement error. The random error was generated using the Box-Muller [5] method. This method produces a user-specified number of normally distributed numbers, which have a user-specified mean and standard deviation. For this investigation the mean was set to zero and the standard deviation to 5 microns (consistent with results in section 2.3). The required number of random numbers were then generated and added to the analytical data. These data were then used as input for the surface fitting programs.

In each surface fitting method, accuracy of the surface point approximation and of surface gradients was checked. Quantification of the error in point estimation and surface gradients is essential for two reasons. The accuracy of an overall knee model is a function of the accuracy of each individual component. More subtly, contact conditions previously have depended on determining collinear normals (dot product of the two normals =-1), or perpendicularity of surface normal and tangent plane (dot

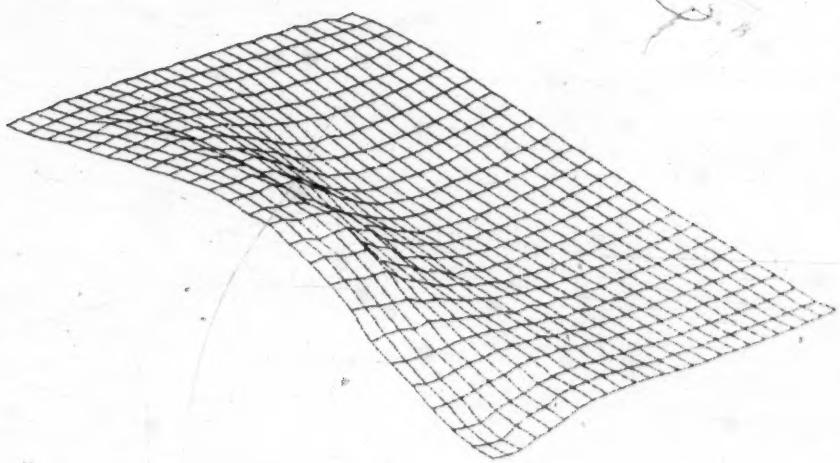

Figure 7. Surface Plot Of Medial Tibia.

product of normal and tangent plane =0). Practically, these conditions cannot be met as explicitly stated; the dot product will not be exactly 0 or -1. Some tolerance ϵ must be determined such that:

$$| 1 + (\vec{n}_1 \cdot \vec{n}_2) | \leq \epsilon \qquad (7)$$

or

$$| \vec{n}_1 \cdot \overline{t} | \leq \epsilon \qquad (8)$$

An analysis of the error in the surface derivatives is fundamental to choosing a realistic and appropriate estimate for the parameter ϵ. Thus the parameter ϵ is the parameter which controls the accuracy of determination of the point of contact, and must be determined by sound methods.

3.2.1 Accuracy of 3-D Points & Directional Derivatives

The effects of smoothing factor and input grid spacing on the magnitude of error in surface point and derivative estimation were investigated. The following function takes into account both errors, and was plotted for various smoothing factors throughout the range from interpolating to least squares splines.

$$T(X,Y) = | Z(X,Y) - S(X,Y) | + | \nabla Z(X,Y) - \nabla S(X,Y) |$$

The function was averaged over numerous points that comprised the middle 90% of the grid in each of the two directions. This process was repeated for input grid spacings of 5mm, 3mm, 1mm, 0.5mm, and 0.25mm. Global minima for the function T(X,Y) were noted for each condyle and grid spacing. The smoothing factor which produced the minimum T(X,Y), as shown in Figures 8&9, was deemed the optimum smoothing factor for that condyle and grid spacing. The parameter T(X,Y) was also investigated for least squares third and fourth order polynomial fits of the hemisphere data.

Tables 1&2 show the average values of T(X,Y) for the three methods used to approximate the hemisphere's surface, for the cases of input data without, and then with simulated error added. The fitting accuracy of the smoothing splines appears more sensitive to the addition of simulated error than the least squares fits. Despite this sensitivity, the average error for the smoothing spline approximation is two to three orders of magnitude smaller than that of either polynomial fit. The values from Tables 1&2 are average values, and thus indicate "global" reduction in error. Average values for $| Z(X,Y) - S(X,Y) |$ and $| \nabla Z(X,Y) - \nabla S(X,Y) |$, the component parts of T(X,Y), are shown in Tables 3-6, and follow similar trends.

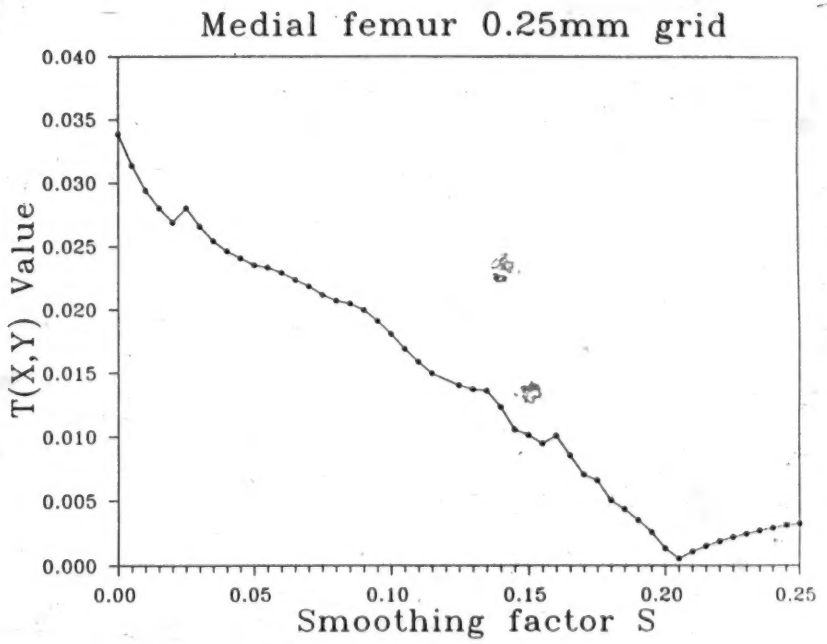

Figure 8. T(X,Y) As A Function Of Smoothing Factor, Medial Femur.

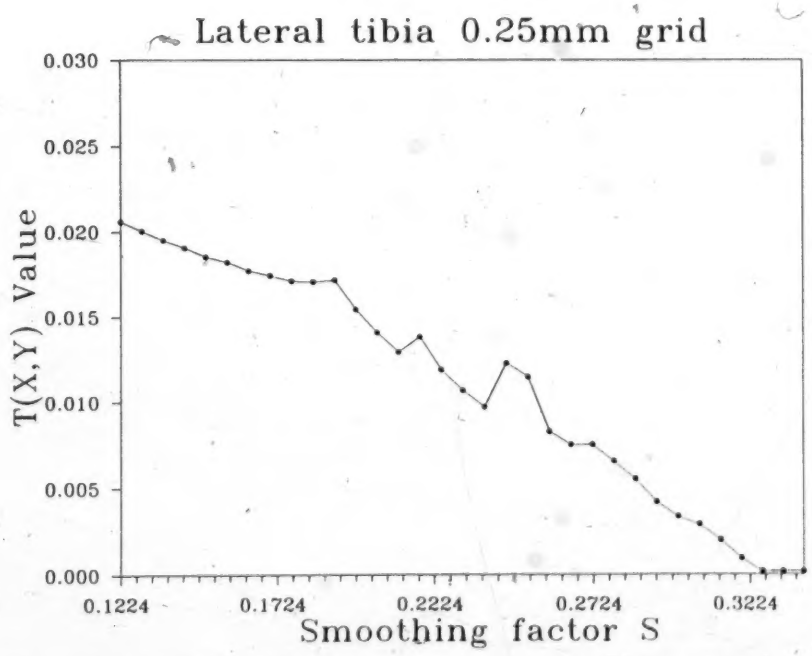

Figure 9. T(X,Y) As A Function Of Smoothing Factor, Lateral Tibia.

Table 1. Average T(X,Y) Value for Hemisphere Surface Approximation (no error added to input data).

Grid Size	Average (X,Y) Value		
	Smoothing Spline	3-rd Order Polynimial	4-th Order Polynomial
5 mm	0.00184	0.97131	0.40432
3 mm	0.00024	0.53459	0.13380
1 mm	0.00007	0.65450	0.20795
.5 mm	0.00011	0.61916	0.21235
.25 mm	0.00019	0.60743	0.19449

Table 2. Average T(X,Y) Value for Hemisphere Surface Approximation (error added to input data).

Grid Size	Average (X,Y) Value		
	Smoothing Spline	3-rd Order Polynimial	4-th Order Polynomial
5 mm	0.00625	0.97147	0.40413
3 mm	0.00299	0.53488	0.13378
1 mm	0.00146	0.65458	0.20792
.5 mm	0.00141	0.61910	0.21291
.25 mm	0.00131	0.60756	0.19449

Table 3. Average Z Error for Hemisphere Surface Approximation (no error added to input data).

Grid Size	Average Z Error (mm)		
	Smoothing Spline	3-rd Order Polynimial	4-th Order Polynomial
5 mm	0.00090	0.8597	0.3457
3 mm	0.00003	0.4629	0.1115
1 mm	0.00003	0.5726	0.1757
.5 mm	0.00003	0.5405	0.1788
.25 mm	0.00003	0.5298	0.1637

Table 4. Average Z Error for Hemisphere Surface Approximation (error added to input data)

Grid Size	Average Z Error (mm)		
	Smoothing Spline	3-rd Order Polynimial	4-th Order Polynomial
5 mm	0.00388	0.8599	0.3455
3 mm	0.00203	0.4632	0.1115
1 mm	0.00086	0.5727	0.1757
.5 mm	0.00076	0.5405	0.1793
.25 mm	0.00069	0.5299	0.1637

Table 5. Average D Error for Hemisphere Surface Approximation (no error added to input data).

Grid Size	Average D Error		
	Smoothing Spline	3-rd Order Polynimial	4-th Order Polynomial
5 mm	0.00095	0.1116	0.05867
3 mm	0.00021	0.07166	0.02233
1 mm	0.00004	0.08191	0.03225
.5 mm	0.00008	0.07866	0.03353
.25 mm	0.00017	0.07763	0.03084

Table 6. Average D Error for Hemisphere Surface Approximation (error added to input data).

Grid Size	Average D Error		
	Smoothing Spline	3-rd Order Polynimial	4-th Order Polynomial
5 mm	0.00236	0.1116	0.05867
3 mm	0.00096	0.07168	0.02233
1 mm	0.00059	0.08192	0.03224
.5 mm	0.00065	0.07865	0.03364
.25 mm	0.00062	0.07766	0.03082

Individual values of T(X,Y) from the smoothing spline without and with simulated error were plotted over one quarter of the hemisphere cross section (as shown in Figure 10)

in Figures 11-20 to investigate "local" variation in the error. Individual values of $| Z(X,Y) - S(X,Y) |$ and $| \nabla Z(X,Y) - \nabla S(X,Y) |$ for spline fits with simulated error were similarly plotted to investigate their local error, and are shown in Figures 21-30. Successive pointwise improvement with finer grid spacing is observed for most points, and the overall maximum error as well as the average error are reduced. The maximum error occurs farthest out from the origin of the grid, where the surface's slope is the greatest.

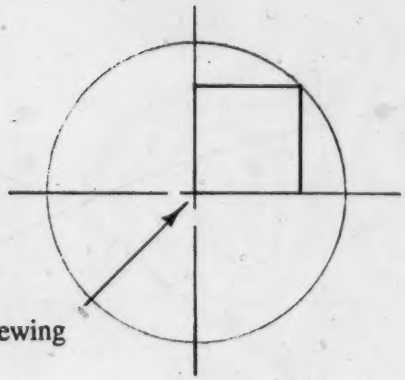

Figure 10. Section Of Quarter Hemisphere For Local Error Examination.

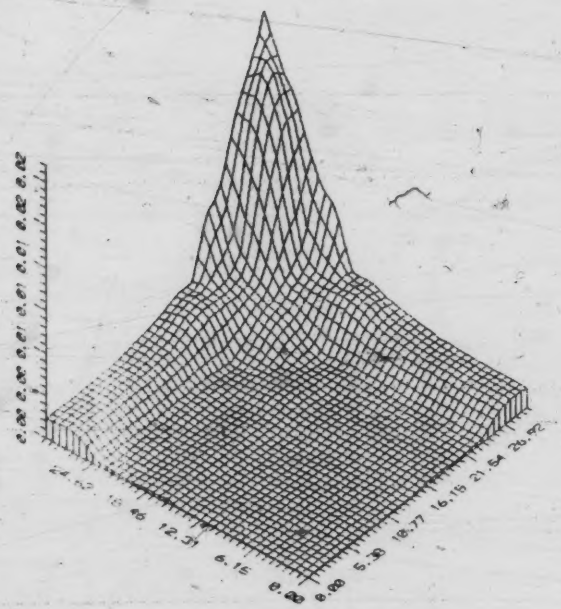

Figure 11. Local T(X,Y) Value On Hemisphere Section Using Smoothing Splines, 5mm Input Grid (no error added to input data).

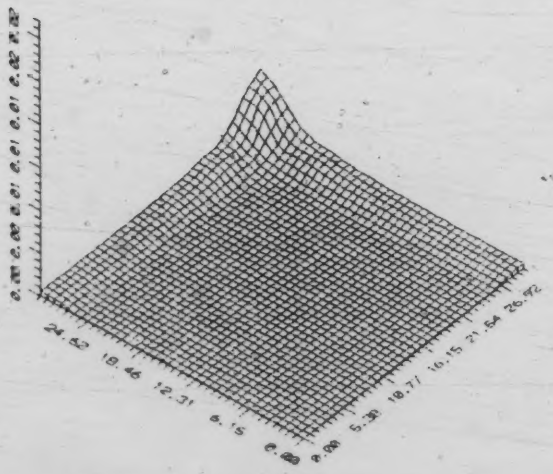

Figure 12. Local T(X,Y) Value On Hemisphere Section Using Smoothing Splines, 3mm Input Grid (no error added to input data).

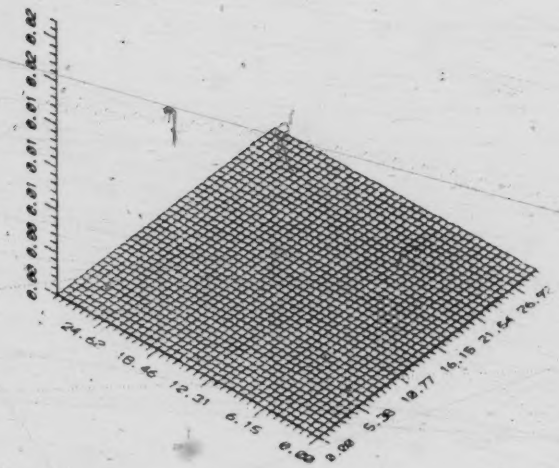

Figure 13. Local T(X,Y) Value On Hemisphere Section Using Smoothing Splines, 1mm Input Grid (no error added to input data).

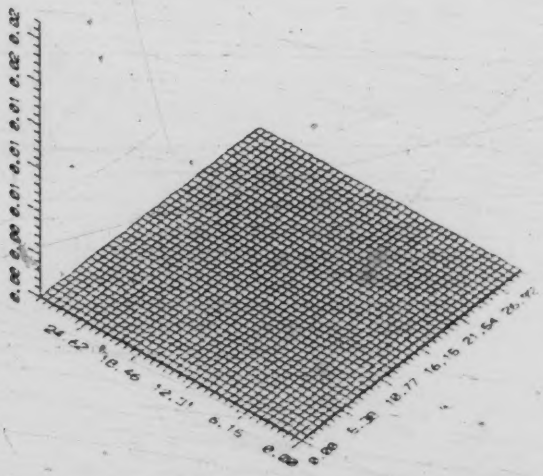

Figure 14. Local T(X,Y) Value On Hemisphere Section Using Smoothing Splines, 0.5mm Input Grid, (no error added to input data).

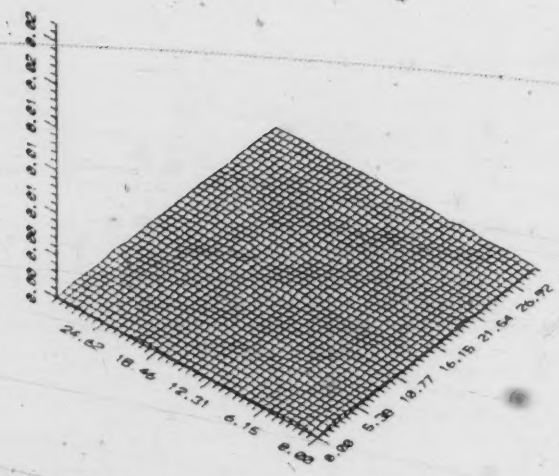

Figure 15. Local T(X,Y) Value On Hemisphere Section Using Smoothing Splines, 0.25mm Input Grid (no error added to input data).

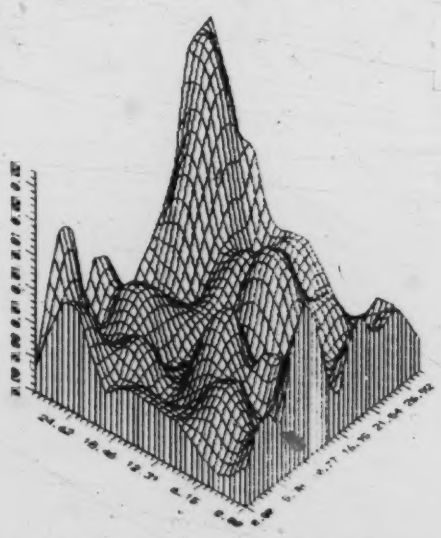

Figure 16. Local T(X,Y) Value On Hemisphere Section Using Smoothing Splines, 5mm Input Grid (error added to input data).

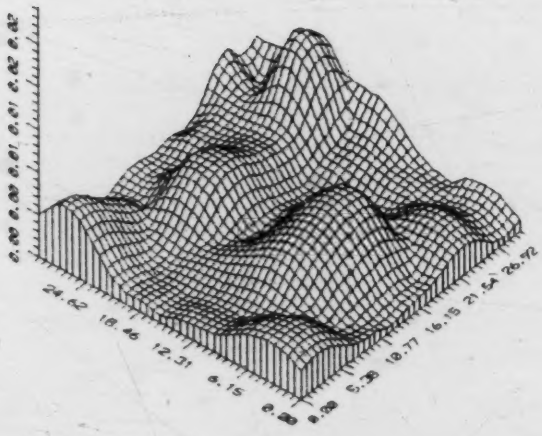

Figure 17. Local T(X,Y) Value On Hemisphere Section Using Smoothing Splines, 3mm Input Grid (error added to input data).

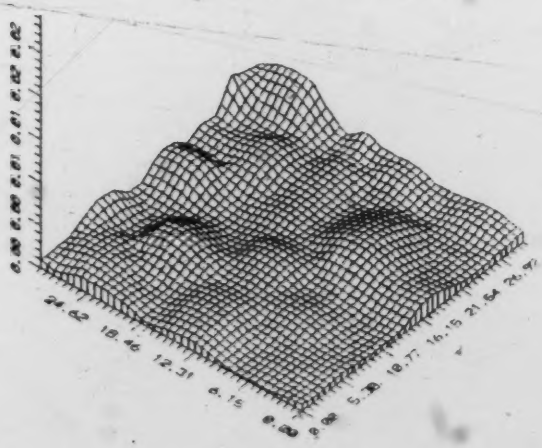

Figure 18. Local T(X,Y) Value On Hemisphere Section Using Smoothing Splines, 1mm Input Grid (error added to input data).

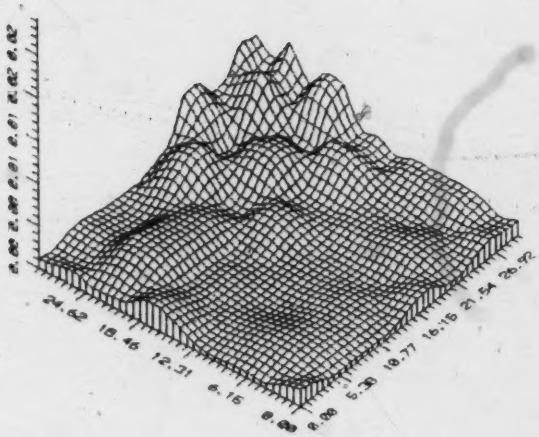

Figure 19. Local T(X,Y) Value On Hemisphere Section Using Smoothing Splines, 0.5mm Input Grid (error added to input data).

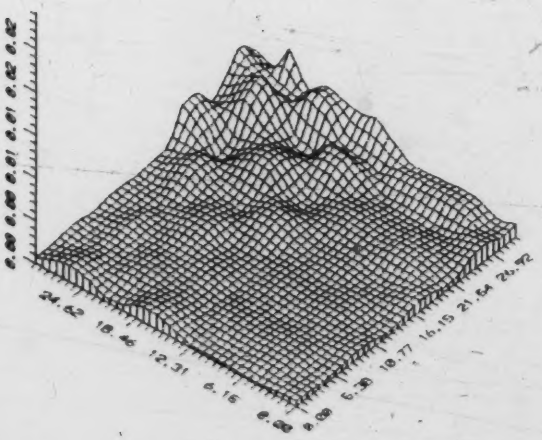

Figure 20. Local T(X,Y) Value On Hemisphere Section Using Smoothing Splines, 0.25mm Input Grid (error added to input data).

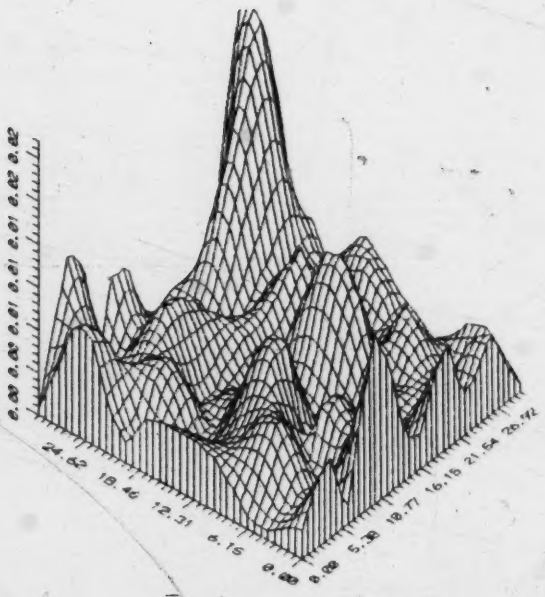

Figure 21. Local Z Error On Hemisphere Section Using Smoothing Splines, 5mm Input Grid (error added to input data).

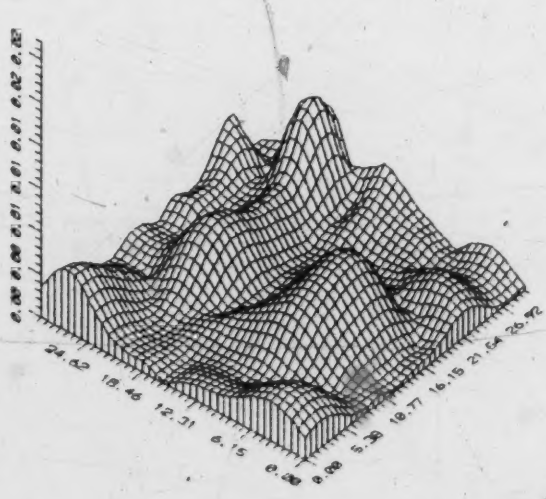

Figure 22. Local Z Error On Hemisphere Section Using Smoothing Splines, 3mm Input Grid (error added to input data).

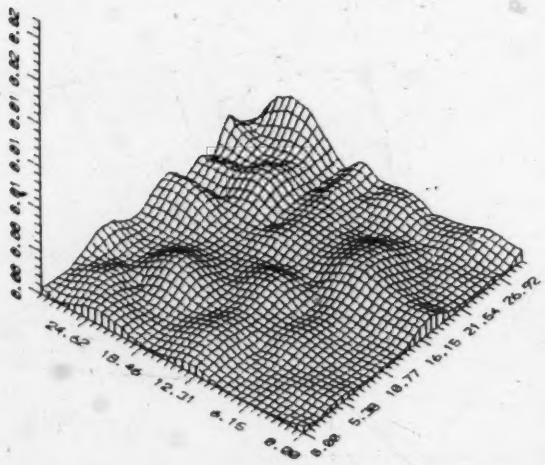

Figure 23. Local Z Error On Hemisphere Section Using Smoothing Splines, 1mm Input Grid (error added to input data).

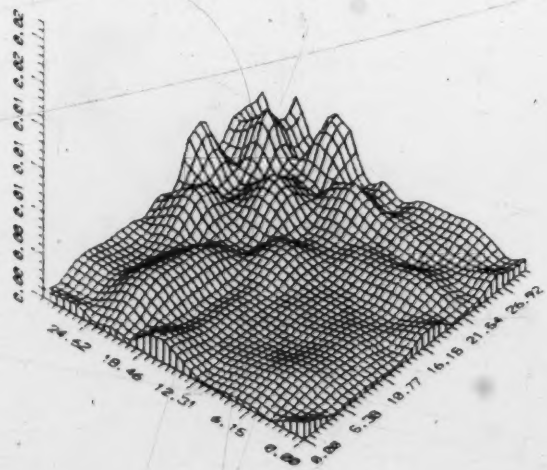

Figure 24. Local Z Error On Hemisphere Section Using Smoothing Splines, 0.5mm Input Grid (error added to input data).

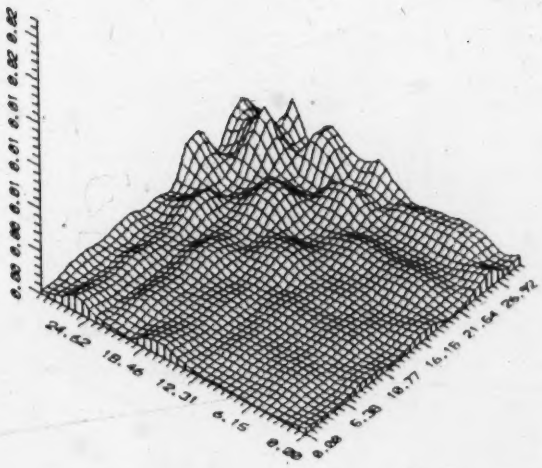

Figure 25. Local Z Error On Hemisphere Section Using Smoothing Splines, 0.25mm Input Grid (error added to input data).

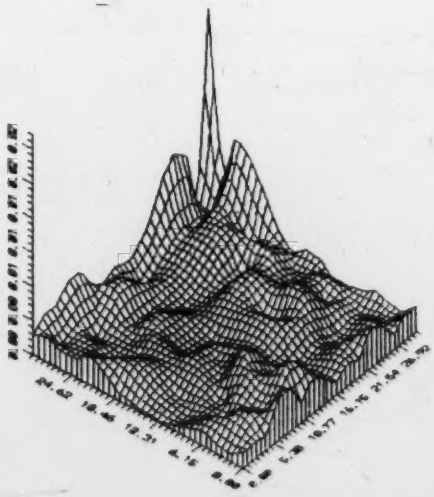

Figure 26. Local D Error On Hemisphere Section Using Smoothing Splines, 5mm Input Grid (error added to input data).

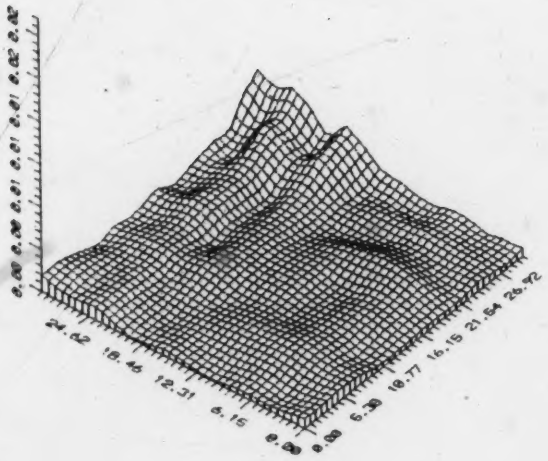

Figure 27. Local D Error On Hemisphere Section Using Smoothing Splines, 3mm Input Grid (error added to input data).

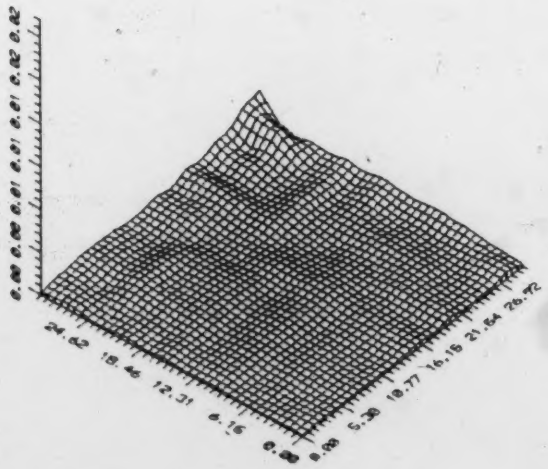

Figure 28. Local D Error On Hemisphere Section Using Smoothing Splines, 1mm Input Grid (error added to input data).

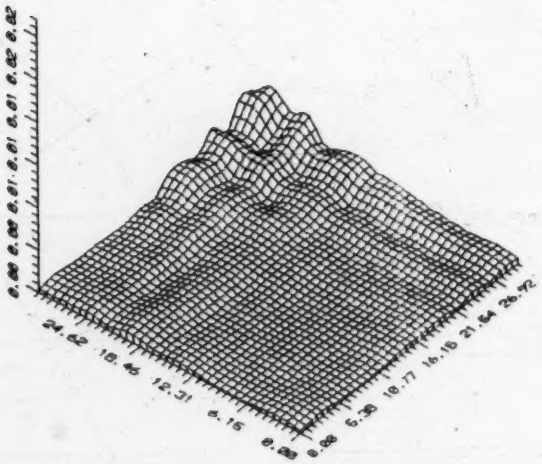

Figure 29. Local D Error On Hemisphere Section Using Smoothing Splines, 0.5mm Input Grid (error added to input data).

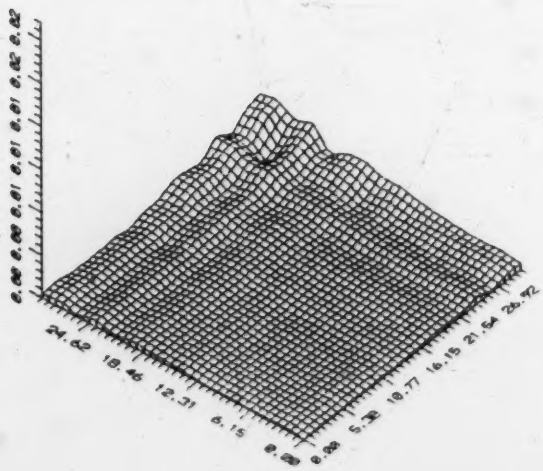

Figure 30. Local D Error On Hemisphere Section Using Smoothing Splines, 0.25mm Input Grid (error added to input data).

Smoothing splines were then used for fitting data generated from the previously mentioned artificial surfaces' polynomial functions. For the case of the tibia, it was observed that a large smoothing factor (a large amount of smoothing) minimized T(X,Y). Conversely it was observed that a small smoothing factor (very little smoothing) minimized T(X,Y) for the femur. The difference is probably due to the greater changes in radius of curvature for the femoral condyles.

Similar to the hemisphere, the accuracy of approximation increased (ie. T(X,Y) decreased) as input grid spacing became finer. These results for the four condyles and five grid spacings are summarized in Tables 7&8. The drawback of finer grid spacing however, is that data base size and program array size quadruple for each halving of input grid spacing, and may be bound by computer hardware. An input grid spacing of 3mm translates to approximately 150 data points, which can be measured within one hour. An input grid spacing of 1mm corresponds to approximately 900 data points, or an estimated 6 hours of measurement, over which operator fatigue, and specimen dehydration would be significant factors. Hence only an automated data acquisition system could be realistically considered for a grid spacing smaller than 3mm.

As previously mentioned, errors in the point estimation and derivative approximation have implications on location of the contact point and contact force. An analysis was performed to determine the region within which contact may occur based on the error in surface coordinate estimation. It was found that the upper limit of the distance to the region's boundary occurred when the radius of curvature was maximum

Table 7. Average Error In Smoothing Spline Approximation of Femoral Condyles.

Grid Size	Lateral Femur			Medial Femur		
	Avg. Z Error (mm)	Avg. D Error	Avg. T(X,Y)	Avg. Z Error (mm)	Avg. D Error	Avg. T(X,Y)
5 mm	.15462	.07821	.23283	.00400	.00195	.00595
3 mm	.00907	.00857	.01764	.00125	.00070	.00195
1 mm	.00154	.00162	.00316	.00040	.00039	.00078
.5 mm	.00068	.00081	.00149	.00037	.00031	.00068
.25 mm	.00039	.00074	.00112	.00027	.00027	.00054

Table 8. Average Error In Smoothing Spline Approximation of Tibial Condyles.

Grid Size	Lateral Tibia			Medial Tibia		
	Avg. Z Error (mm)	Avg. D Error	Avg. T(X,Y)	Avg. Z Error (mm)	Avg. D Error	Avg. T(X,Y)
5 mm	.00203	.00059	.00262	.00220	.00068	.00288
3 mm	.00093	.00035	.00128	.00105	.00030	.00135
1 mm	.00039	.00021	.00059	.00047	.00020	.00067
.5 mm	.00014	.00006	.00020	.00016	.00007	.00023
.25 mm	.00014	.00004	.00018	.00012	.00005	.00017

and the slope minimum. These maxima are summarized in Table 9. These values suggest that on average, the actual contact point will be within a 1mm of the calculated contact point (with two exceptions for the lateral femur). Hence when determining the moment of the contact force about any point, the moment arm can be expected to be uncertain to less than 1mm due to the fitting method (with the same two exceptions). A similar calculation was performed using 0.5mm for the allowable deviation in Z coordinate values (0.5mm = the "standard deviation" cited previously in the Wismans model), and yielded possible contact radius of 7.73mm.

The other contact criterion, collinearity of surface normals at the contact point, must also be considered. Error in the slope of the surface will affect the direction of the surface normal. Hence opposing tibial and femoral normals may not be collinear at the contact point due to error in the slope estimation alone. Since error in the slope of the surfaces was investigated, an upper limit on this non-collinearity can be determined. The worst case would be the combined maxima of slope errors on opposing condyles. The arctangent of the average error plus three standard deviations (giving a 99.74% confidence interval) was calculated, and represents the maximum expected uncertainty of contact point normals. This calculation was done for both lateral and medial condyles, for all 5 input grid spacings. The resulting error angles and their cosines are summarized in Table 10. Thus it is now possible to put realistic limits on ϵ in equations (7) and (8).

Equation (7) idealizes two opposing, perfectly collinear vectors, the dot product of which would be -1 exactly. Using the maximum expected errors from Table 10, it

is clear that the bound to this dot product is cos(180°- error angle), or -0.97894 in the worst case (lateral contact, 5mm input grid). This gives an upper bound of 0.0211 for ϵ in equation (7) if a 5mm input grid is used.

Equation (8) idealizes a vector intersecting a plane at a right angle, the dot product of which would be 0 exactly. Again using maximum expected errors from Table 10 it is clear that the lower bound to this dot product is cos(90°- error angle), or 0.2042 in the worst case (lateral contact, 5mm input grid). Hence ϵ of equation (8) has a maximum value of 0.2042 if the contact criterion is expressed in this manner.

If a 3mm input grid spacing is used, the maximum value of ϵ in equation (7) becomes 0.00032, and the maximum of ϵ in equation (8) becomes 0.0253. The reduction in these values is not as significant for increasingly finer input grids.

3.2.2 Application To Cadaver Specimens

This method was experimentally tested on a cadaveric specimen. The cadaveric specimen was obtained in a frozen state, and subsequently thawed in a refrigerator for 48 hours. Excess soft tissue was trimmed off and the joint dis-articulated by an orthopaedic surgeon who performed the dissection. The ligaments and menisci were removed at their attachment points. Half inch holes were bored approximately one inch deep into the ends of the specimens, and threaded studs bonded within these holes using bone cement. After the bone cement had set, the specimens were mounted and stored in a refrigerator with a moist cloth over them until digitizing took place. The specimens were misted lightly with a saline solution about every ten minutes while in the digitizer.

The articular joint surfaces showed visual evidence of arthritis in the form of inflammation and small abraded patches. There was no visually detected deformation of healthy cartilage under the force applied by the digitizer probe before coordinate measurement occurred. This was not the case with the abraded patches though; the probe tip disappeared inside the abraded surface before sufficient force was generated to cause automatic data acquisition. Thus it is the author's opinion that cadaveric specimens showing evidence of arthritis are unsuitable for digitizing in this manner.

Table 9. Maximum Distance To Contact Region Boundary For Various Input Grid Spacings.

Grid Size	Maximum Distance To Contact Region Boundary (mm)			
	Lat. Tibia	Med. Tibia	Lat. Femur	Med. Femur
5 mm	0.533	0.593	4.30	0.551
3 mm	0.360	0.410	1.04	0.308
1 mm	0.233	0.273	0.430	0.173
.5 mm	0.141	0.160	0.270	0.168
.25 mm	0.138	0.137	0.220	0.142

Table 10. Normal Vector Error Angle.

Grid Size	Lateral Contact		Medial Contact	
	Combined Error Angle(°)	Angle Cosine	Combined Error Angle(°)	Angle Cosine
5 mm	11.78	0.97894	0.3881	0.99998
3 mm	1.452	0.99968	0.1874	0.99999
1 mm	0.2946	0.99998	0.1328	0.99999
.5 mm	0.1659	0.99999	0.0675	0.99999
.25 mm	0.1328	0.99999	0.0618	0.99999

Chapter Four

4.0 Conclusions

In this investigation methods for obtaining precise three dimensional coordinates from cadaveric specimens, and for processing these coordinates in a manner useful to a comprehensive knee model were determined. Toward this goal, devices for positioning the digitizer used to within its resolution, and for rigidly securing the specimen during digitization were developed. The effect of the amount of input data on surface fitting accuracy was investigated, and it was found that the accuracy and also computational time required to complete the fitting increased with decreasing input grid spacing (more input data).

Smoothing spline fitting was found to be an extremely accurate method for fitting three dimensional surfaces to digitized data. Using this method it was possible to estimate surface coordinates to less than 1 micron uncertainty, on average. Error in surface slope, and its effect on the location of the tibio-femoral contact point were also investigated. These errors were found to produce an uncertainty in the location of the contact point of (on average) less than 1mm. The error in surface slope was also used to quantify reasonable bounds on non-collinearity of surface normals at the contact point.

Moisture loss from the specimen during the digitization is an important consideration. Maximizing grid spacing minimizes digitizing time, but at the expense of fitting accuracy. However, minimizing grid spacing results in more time required for digitizing, leading to more moisture loss from the specimen, and thus changes in the surface shape as the articular cartilage dries out. Some literature does exist on moisture

loss as a function of time, and the specimens were periodically misted with a saline solution during digitization to minimize moisture loss. Further investigations could be performed to determine rate of surface deformation with moisture loss, since a highly precise digitizer is easily accessible. It is also recommended that digitizing be completed within 24 hours of specimen dissection (post thawing), and that the specimen be stored in a cool humid environment between dissection and digitization.

To the author's knowledge no other researchers have conducted a sensitivity analysis of their models to the method of surface description, or the accuracy of surface description. Once this method has been incorporated into a complete knee model, the sensitivity of results to accuracy of surface description should be investigated further. This would perhaps lend a better insight into consequences of amount of input data on global results, and thus weight the tradeoff between longer digitizing time and amount of data required.

REFERENCES

1.) An K.N., Kwak B.M., Chao E.Y., Morrey B.F., "Determination of Muscle and Joint Forces: A New Technique to Solve the Indeterminate Problem", Transactions of the ASME, Vol. 106, 364-367, 1984.

2.) Andriacchi T.P., Mikosz R.P., Hampton S.J., Galante J.O., "A Statically Indeterminate Model of the Human Knee Joint", Proc. Biomech. Symp., AMV-23, 227-229, 1977.

3.) Baragar F.A., Osborn J.W., "Efficiency as a Predictor of Human Design in the Sagittal Plane", J. Biomech., Vol. 20, 447-457, 1987.

4.) Boresi A.B., Sidebottom O.M., Advanced Strength of Materials, 4-th Edition, John Wiley & Sons, 1985.

5.) Box G.E.P., Muller M.E., "A Note on the Generation of Random Normal Deviates", Annals of Math. Stat., Vol. 29, 610-611, 1958.

6.) Chand R., Haug E., Rim K., "Stress in the Human Knee Joint", J. Biomech., Vol. 9, 417-422, 1976.

7.) Dierckx P., "An Algorithm for Least Squares Fitting of Cubic Spline Surfaces to Functions on a Rectilinear Mesh Over a Rectangle", J. Comput. & Applied Math., Vol. 3, 113-129, 1977.

8.) Dierckx P., "A Fast Algorithm for Smoothing Data on a Rectangular Grid While Using Spline Functions", SIAM J. Numer. Anal., Vol. 19, 1286-1303, 1982.

9.) Dierckx P., "FITPACK: Surface Fitting Routines", Report TW-122, June 1989, Dept. of Comp. Sci., Celestijnenlaan 200A B-3030 Leuven (Belgium) Fax. +32 16 20 53 08.

10.) Elvis P.R., "Examining Static Loading & Experimental Yielding: Linearized Incremental Variable Expression Systems", Act. Artic. No., Vol. 42, 1935-1977.

11.) Ewing J.W., "Articular Cartilage & Knee Joint Function", Basic Science & Arthroscopy, Raven Press, New York, 1-18, 1988.

12.) Farin G., Curves & Surfaces for Computer Aided Geometric Design, Academic Press Inc., 1988.

13.) Frank C., Personal correspondence with Dr. Cy Frank, Orthopaedic surgeon, Foothills Hospital, Calgary Alberta, Canada.

14.) Frankel V.H., Burstein A.H., Brooks D.B., "Biomechanics of Internal Derangement of the Knee", J. Bone & Joint Surg., Vol. 53-A, 945-962, 1971.

15.) Ghosh S.K., "A Close Range Photogrammetric System for 3-D Measurements & Perspective Diagramming in Biomechanics", J. Biomech., Vol. 16, 667-674, 1983.

16.) Goodfellow J., O'Connor J., "The Mechanics of the Knee and Prosthesis Design", J. Bone & Joint Surg., Vol. 60-B, 358-369, 1978.

17.) Hefzy M.S., Grood E.S., "Review of Knee Models", Applied Mechanics Reviews, Vol.41, 1-13, 1988.

18.) Iseki F., Tomatsu T., "The Biomechanics of the Knee Joint With Special Reference to the Contact Area", Keio. J. Med., Vol. 25, 37-44, 1976.

19.) Jacobson A., Caufield P.W., Introduction to Radiographic Cephalometry, Lea & Febiger, Philadelphia, 1985.

20.) Kapandji I.A., The Physiology of the Joints, Volume Two: The Lower Limb, 5-th Edition, Churchill Livingston, New York, 1987.

21.) Lindahl O., Movin A., "The Mechanics of Extension of the Knee Joint", Act. Orthop. Scand., Vol. 38, 226-234, 1967.

22.) Maquet P., "Biomechanics & Osteo-arthritis of the Knee", S.I.C.O.T., XIe Congress, Mexico, 1969, Imprimerie des Sciences, Bruxelles, 317-357, 1970.

23.) Markolf K.L., Mensch J.S., Amstutz H.C., "Stiffness and Laxity of the Knee: The Contribution of the Supporting Structures", J. Bone & Joint Surg., Vol. 58-A, 583-593, 1976.

24.) Matthews L., Sonstegard D., Henke J., "Load Bearing Characteristics of the Patello-femoral Joint", Act. Orthop. Scand., Vol. 48, 511-516, 1977.

25.) Mikosz R.P., Andriacchi T.P., Andersson G.B.J., "Model Analysis of Factors Influencing the Prediction of Muscle Forces at the Knee", Journal of Orthopaedic Research, Vol. 6, 205-214, 1988.

26.) Miller I., Freund J.E., Probability & Statistics for Engineers, 3-rd Edition, Prentice-Hall, New Jersey, 1985.

27.) Murray D.G., "Total Knee Arthroplasty", Clinical Orthopaedics & Related Research, No. 192, pp.59, Jan/Feb 1985.

28.) Osborn J.W., Baragar F.A., "Predicted Pattern of Human Muscle Activity During Clenching", J. Biomech., Vol. 11, 389-395, 1978.

29.) Press W.H., Flannery B.P., Teukolsky S.A., Numerical Recipes, The Art of Scientific Computing,Cambridge University Press, New York, 1986.

30.) Radin E.L., Paul I.L., "A Consolidated Concept of Joint Lubrication", J. Bone & Joint Surg., Vol. 54-A, 607-616, 1972.

31.) Rehder U., "Morphometric Studies on the Symmetry of the Human Knee Joint: Femoral Condyles, J. Biomech., Vol. 16, 351-361, 1983.

32.) Reilly D.T., Martens M., "Experimental Analysis of the Quadriceps Muscle Force & Patello-femoral Joint Reaction Force for Various Activities", Act. Orthop. Scand., Vol. 43, 126-137, 1972.

33.) Thomas G., Finney R.L., Calculus & Analytic Geometry, 6-th Edition, Addison Wesley, 1984.

34.) Wismans J., Veldpaus F., Janssen J., Huson A., Struben P., "A Three Dimensional Mathematical Model of the Knee Joint", J. Biomech., Vol. 13, 677-685, 1980.

35.) Wongchaisuwat C., Hemami H., Buchner H.J., "Control of Sliding and Rolling at Natural Joints, Transactions of the ASME, Vol. 106, 368-375, 1984.

36.) Wyss U.P., Doerig M., Frey O., Gschwend N., "Dimensions of the Femoral Condyles", Biomechanics: Principles & Applications, 291-297, 1982.

37.) Zoghi M., Hefzi M.S., Fu K.C., "A Three Dimensional Geometrical Model of the Distal Human Femur", Advances in Bioengineering, 1989.

APPENDIX

Calcluation for maximum distance to contact region boundary:

The purpose of this analysis is to determine the region around a given surface point (point 1) within which contact may occur based on the error in surface coordinate estimation. Contact implies that two points on opposing condyles physically touch. Thus it is necessary to determine the distance from the given point for which the change in the Z coordinate is equal to the uncertainty in estimating that coordinate. The uncertainty in estimating the coordinate appears in Tables 7&8 as the average Z error, and is referred to in this analysis as ΔZ. Hence the problem is to determine the length ℓ in the diagram below such that $| Z_{point\ 1} - Z_{point\ 2} |$, the difference in elevation between the two points, is at most ΔZ. The curve with radius of curvature r represents the surface of a condyle.

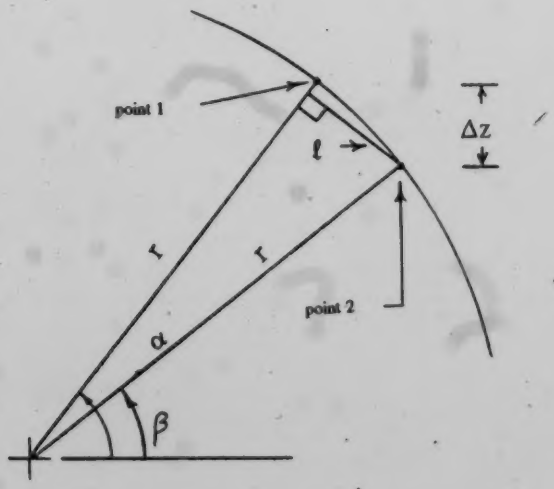

From the diagram it is clear that length ℓ can be expressed:

$$\ell = r \sin (\alpha - \beta) = r [\sin\alpha \cos\beta - \cos\alpha \sin\beta] \quad (1)$$

and also that the difference ΔZ can be written as:

$$r \sin\alpha - r \sin\beta = \Delta z$$

thus

$$\sin\beta = \sin\alpha - (\Delta z)/r \qquad (2a)$$

and then using a right triangle:

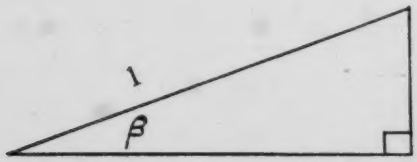

$$\sin\alpha - \frac{\Delta z}{r}$$

it can be shown that:

$$\cos\beta = \sqrt{1 - (\sin\alpha - \frac{\Delta z}{r})^2} \qquad (2b)$$

now, using (2a) and (2b) in (1) yields:

$$\ell = r \sin\alpha \left(\sqrt{1 - (\sin\alpha - \frac{\Delta z}{r})^2} - \cos\alpha \right) + \Delta z \cos\alpha$$

This equation was evaluated through α=5° to 90° using:

$$r = r_{min} + (r_{max} - r_{min}) \left(\frac{\alpha - 5°}{85°} \right)$$

to account for variation in the radius of curvature along the condyle, with values for r_{min} and r_{max} taken from literature [20]. The maximum value for ℓ through this range for each condyle and grid spacing was recorded and appears in Table 9.

Calculation of error in normal vector:

Tangent vectors in the x and y directions can be written:

$$\vec{t}_x = 1\ \vec{i} + 0\ \vec{j} + m_x\ \vec{k}$$

$$\vec{t}_y + 0\ \vec{i} + 1\ \vec{j} + m_y\ \vec{k}$$

where m_x and m_y are the slopes (derivatives) in the x and y directions respectively. The normal vector is the cross product of the tangents, namely:

$$\vec{n} = \vec{t}_x \times \vec{t}_y$$

or, rewriting:

$$\vec{n} = -m_x\ \vec{i} - m_y\ \vec{j} + 1\ \vec{k}$$

for which the error in the normal is:

$$(\varepsilon_{\vec{n}})^2 = \left(\frac{\partial \vec{n}}{\partial m_x}\varepsilon_{m_x}\right)^2 + \left(\frac{\partial \vec{n}}{\partial m_y}\varepsilon_{m_y}\right)^2$$

$$= (-1\ \varepsilon_{m_x})^2 + (-1\ \varepsilon_{m_y})^2$$

$$= (\varepsilon_{m_x})^2 + (\varepsilon_{m_y})^2$$

$$\varepsilon_{\vec{n}} = [(\varepsilon_{m_x})^2 + (\varepsilon_{m_y})^2]^{0.5} \qquad (3)$$

Equation (3) represents the second term in the error function T(X,Y), namely $|\ \nabla Z(X,Y) - \nabla S(X,Y)\ |$, which was evaluated and averaged over many points within

the fitting domain, and is referred to as the average D error in this text.

Least Squares Polynomials:

The following expressions were used for the polynomial fits:

4-th order:

$$z(x,y) = \beta_0 + \beta_1 x + \beta_2 y + \beta_3 x^2 + \beta_4 y^2 + \beta_5 xy + \beta_6 x^3 + \beta_7 y^3 + \beta_8 x^2 y + \beta_9 x y^2 + \beta_{10} x^4 + \beta_{11} y^4 + \beta_{12} x y^3 + \beta_{13} x^2 y^2 + \beta_{14} x^3 y$$

3-rd order:

$z(x,y)$= terms β_0 through β_9 of the above expression

These expressions were fitted to the 3-dimensional data for the hemisphere, and condyle surfaces using the method described by Miller & Freund [26].